





Goal-Oriented Adaptive Finite Element Multilevel Monte Carlo with Convergence Rates

Joakim Beck ^{a,1}, Yang Liu ^{a,1,*}, Erik von Schwerin ^{a,1}, Raúl Tempone ^{a,1,2}


^a*Computer, Electrical and Mathematical Sciences and Engineering,
4700 King Abdullah University of Science and Technology (KAUST),
Thuwal 23955-6900, Kingdom of Saudi Arabia*

Abstract

In this study, we present an adaptive multilevel Monte Carlo (AMLMC) algorithm for approximating deterministic, real-valued, bounded linear functionals that depend on the solution of a linear elliptic PDE with a lognormal diffusivity coefficient and geometric singularities in bounded domains of \mathbb{R}^d . Our AMLMC algorithm is built on the results of the weak convergence rates in the work [Moon et al., BIT Numer. Math., 46 (2006), pp. 367–407] for an adaptive algorithm using isoparametric d-linear quadrilateral finite element approximations and the dual weighted residual error representation in a deterministic setting. Designed to suit the geometric nature of the singularities in the solution, our AMLMC algorithm uses a sequence of deterministic, non-uniform auxiliary meshes as a building block. The above-mentioned deterministic adaptive algorithm generates these meshes, corresponding to a geometrically decreasing sequence of tolerances. In particular, for a given realization of the diffusivity coefficient and accuracy level, AMLMC constructs its approximate sample using the first mesh in the hierarchy that satisfies the corresponding bias accuracy constraint. This adaptive approach is particularly useful for the lognormal case treated here, which lacks uniform coercivity and thus produces functional outputs that vary over orders of magnitude when sampled. Furthermore, we discuss iterative solvers and compare their efficiency with direct ones. To reduce computational work, we propose a stopping criterion for the iterative solver with respect to the quantity of interest, the realization of the diffusivity coefficient, and the desired level of AMLMC approximation.

From the numerical experiments, based on a Fourier expansion of the diffusivity coefficient field, we observe improvements in efficiency compared with both standard Monte Carlo (MC) and standard MLMC (SMLMC) for a problem

*Corresponding author

Email address: yang.liu.3@kaust.edu.sa (Yang Liu )

¹KAUST SRI Center for Uncertainty Quantification in Computational Science and Engineering

²Alexander von Humboldt Professor in Mathematics for Uncertainty Quantification, RWTH Aachen University, 52062 Aachen, Germany.

with a singularity similar to that at the tip of a slit modeling a crack.

Keywords: Multilevel Monte Carlo, Goal-oriented adaptivity, Computational complexity, Finite elements, Partial differential equations with random data, Lognormal diffusion

2020 MSC: 65C05, 65N50, 65N22, 35R60

1. Introduction

Motivated by the importance of uncertainty quantification on random partial differential equations (RPDEs) [20, 59, 72], we consider the adaptive computation and error control for quantities of interest (QoIs) of the form $\mathbb{E}[Q(u)]$, where Q is a deterministic, real-valued, bounded linear functional of the stochastic solution u to a class of linear elliptic PDE with random coefficients,

$$-\nabla \cdot (a(\mathbf{x}; \omega) \nabla u(\mathbf{x}; \omega)) = f(\mathbf{x}; \omega) \quad \text{for } \mathbf{x} \in \mathcal{D}, \quad (1a)$$

$$u(\mathbf{x}; \omega) = 0 \quad \text{for } \mathbf{x} \in \partial\mathcal{D}_1, \quad (1b)$$

$$\partial_n u(\mathbf{x}; \omega) = 0 \quad \text{for } \mathbf{x} \in \partial\mathcal{D} - \partial\mathcal{D}_1, \quad (1c)$$

where the differential operators, $\nabla \cdot$ and ∇ , are taken with respect to the spatial variable, \mathbf{x} , and ∂_n is the outward normal derivative operator. Here, ω corresponds to a complete probability space $(\Omega, \mathcal{F}, \mathbb{P})$. With respect to the spatial domain \mathcal{D} , suppose it is an open and bounded polygonal/polyhedral domain in \mathbb{R}^d , $d \geq 2$ with boundary $\partial\mathcal{D}$. The boundary \mathcal{D} splits into its Dirichlet and Neumann parts, and we consider each part as the union of a finite number of intervals or polygons. Naturally, the solution u is stochastic because of the randomness induced by the stochastic diffusivity coefficient field $a(\mathbf{x}; \omega)$ and/or the stochastic forcing $f(\mathbf{x}; \omega)$. Using properly-refined discretizations by isoparametric d-linear quadrilateral finite elements, we propose the development and analysis of an adaptive multilevel Monte Carlo (AMLMC) algorithm to approximate $\mathbb{E}[Q(u)]$ with error control.

An error expansion with a computable leading order term that is asymptotically accurate guides our AMLMC stochastic refinements. First developed in [65], this error expansion uses a dual weighted error representation and yields an error density.

The error density characterizes the optimality of refined meshes and the resulting complexity of AMLMC. It also provides insight into the comparison with MLMC using uniform discretizations, thus motivating the class of problems where AMLMC provides a computational advantage. A specific challenge to address in this work is the lognormal distribution in the diffusivity coefficient, a , which implies that (1) lacks uniform coercivity, cf. [5]. Thus, it maps to functional outputs that extensively vary, a particularly challenging feature that requires addressing using stochastic discretizations.

The analysis of the finite element method (FEM) with uniform meshes for numerically approximating PDEs is well established. See e.g. the books [6, 12, 30,

69, 78]. FEM is a major numerical method for solving PDEs because of its accuracy, efficiency, stability, and versatility. However, isotropic or anisotropic, uniform meshes are not always optimal. For instance, for singularities induced by the problem geometry or when considering PDEs with highly spatially-varying coefficients, there are h-adaptive [2, 3, 16, 29, 52, 65, 71, 74, 75, 77, 81, 82] and hp-adaptive [1, 25, 70, 73, 83] strategies, based on local error indicators, which result in higher accuracies through the efficient allocation of the degrees of freedom (DoF) in the meshes. When approximating $\mathbb{E}[Q(u)]$, it is preferable to adapt the mesh with respect to the error of approximating this scalar QoI rather than the whole PDE solution. This approach is known as goal-oriented adaptivity [76, 79, 91]. Our aim is to pursue goal-oriented adaptivity for multi-level Monte Carlo. For our approach, the class of coefficients requires sufficient pathwise regularity. Problems whose coefficients are almost surely and everywhere rough must be treated with other techniques and are outside the scope of this study, see for example [40], which studies approximation using uniform discretizations.

Heinrich [42, 43] introduced multilevel Monte Carlo for applications to parametric integration. Motivated by applications in computational finance, Keibaier [51] introduced a two-level control variate technique in Monte Carlo (MC) sampling for the weak approximation of stochastic differential equations (SDEs). Giles [33] extended this approach to the now-famous multilevel Monte Carlo (MLMC) using a full hierarchy of discretizations with geometrically decreasing grid sizes. By optimally selecting the number of samples on each level and sampling more from coarse, inexpensive levels, and less from fine, expensive levels, the MLMC method decreases the computational cost. This cost reduction with respect to single-level MC usually goes beyond a constant factor, unlike the cost reduction of standard control variate techniques. MLMC can reduce the computational complexity to compute a solution with an error tolerance $TOL > 0$, cf. Theorem 1. Central limit results are useful for estimating and controlling the statistical error in the MLMC in terms of its variance. These results, cf. [14, 22] and the generalization in [45], are applications of the Lindeberg central limit theorem because the MLMC samples are not identically distributed across levels.

To achieve the optimal MLMC complexity rate, sufficiently accurate estimates of the variance on each level and the bias on the deepest level are required.

To preserve the theoretical complexity, any practical MLMC algorithm must produce variance and bias estimates without incurring considerable overhead cost. Giles proposed an algorithm [33] that addresses this by successively increasing the number of levels and producing sample variance estimates across levels and the corresponding bias. His approach uses an arbitrarily fixed accuracy splitting between the bias and the statistical errors. This choice appears in similar versions elsewhere in the literature, see [21, 32, 35, 89]. Alternatively, the continuation MLMC (CMLMC) algorithm, proposed in [22], calibrates models for variance and weak convergence, and the average computational work per sample. The CMLMC algorithm solves the given problem for a sequence of

decreasing tolerances, ensuring that the cost of the sequence of problems is dominated by the expense of the problem we originally intended to solve. Thus, tolerance is the continuation parameter here, and the algorithm stops when the critical error tolerance is achieved with a prescribed high probability level. Creating this auxiliary sequence of smaller problems enhances the learning of all necessary parameters to efficiently run MLMC and optimize the bias and variance contributions to minimize the computational work. The area of MLMC methods is still very active. See [34] for a broader view.

MLMC has been successful in RPDEs. Considerable attention has been devoted to controlling the error in the challenging case of a lognormal distribution in the diffusivity coefficient, a , cf. (1a). Error estimates have been presented for the numerical approximation of solutions, or functionals thereof, to elliptic PDEs with random coefficients [11, 17–19, 21, 40, 89] with varying assumptions, in particular related to the random diffusivity coefficient, physical domain, and boundary conditions. Lognormal coefficient fields are considered in [11] for the case of full spatial regularity and uniform coercivity of the random field, and in [17–19, 21] for limited spatial regularity and without assuming uniform coercivity. Teckentrup et al. [89] extended the error analysis provided by Charrier et al. [19] to address challenges because of non-smooth physical domains. For MLMC, Charrier et al. [19] derived uniform error bounds for approximating the expectation of a smooth functional of the random solution in \mathcal{C}^2 bounded Lipschitz domains. MLMC convergence results have been derived for real-valued, bounded linear functionals of the random solution of elliptic problems on $[0, 1]^d$ domains using Dirichlet boundary conditions in [21] and on particular types of non-smooth domains in [89]. Teckentrup et al. [89, Theorem 2.3] show that there is an optimal work convergence rate that is similar to the previously mentioned complexity rates, cf. Theorem 1, but depends on the relation between the rate of variance convergence of the discretization method of the underlying equation and work complexity associated with generating a single sample of the quantity of interest. In certain cases, the computational complexity is of the optimal rate, namely $\mathcal{O}(\text{TOL}^{-2})$.

Multilevel Quasi-Monte Carlo (MLQMC) methods with uniform mesh refinements have been proposed in [36, 44, 54] and are outside the scope of this study.

Within MLMC, the notion of adaptivity takes different forms. For instance, we may optimally distribute the MLMC hierarchy, an issue that remains relevant even for uniform discretization. Thus, [39] contains a general optimization of the MLMC parameters in the discretization hierarchy, especially the separation of levels and optimized the accuracy of budget allocation between the bias and the statistical errors. In MLMC, we may consider adaptively selecting the time-stepping method to save computational work. This is demonstrated in [15, 66, 67] in the context of stochastic reaction networks. The notion of adaptivity exploited in this work is the mesh size control. Here, the step size or the mesh size is selected to minimize cost while achieving a prescribed accuracy. The work [46, 47] first introduced MLMC stepsize goal-oriented adaptivity for Itô SDEs, defining the MLMC levels in terms of accuracy requirements achieved by

a suitable adaptive algorithm, rather than in terms of uniform discretizations. This idea is general and is also useful in MLMC for RPDEs.

Eigel et al. [27], the closest reference to this work, used goal-oriented adaptivity in the context of MLMC for (1), assuming uniform coercivity, an assumption for which in this work we relax to treat the lognormal case. Their approach differs from ours because (i) it is based on batch adaptivity, (ii) the error indicators are different, do not yield an error density, and seem less sharp, cf. [61], (iii) they based their error control on the MSE error and did not separate the statistical error and bias errors as we did. On a less related note, Scarabosio et al. [85] used goal-oriented model adaptivity based on a hierarchical control variate using two and three levels. They based their error estimates on verifying the current model output pathwise against a higher-fidelity model. For adaptive MLMC using norm error control we refer to [53] and the PhD thesis [93]. The goal in those studies was to perform pathwise adaptivity for functional approximation for the expected value of the solution and not to compute a quantity of interest as we do here. The more recent work [55] is focused on adaptivity with multilevel stochastic collocation for solving elliptic PDEs with random data by combining adaptive (anisotropic) sparse Smolyak grid approximations in the stochastic space, using the Sparse grid Matlab kit (version 17-5) [80], for each collocation point by applying the dual weighted residual method [13] for spatial goal-oriented adaptive mesh refinements.

Our contributions in this work are as follows: we propose a novel AMLMC for (1) with geometric singularities and a lognormal random diffusivity coefficient. We build our AMLMC on [65], which developed weak convergence rates for an adaptive algorithm using isoparametric d-linear quadrilateral finite element approximations and the dual weighted residual error representation in a deterministic setting. This provides us with sharp error estimates and indicators for creating locally refined sequences of meshes tuned to the geometry-driven singularity at hand. Compared with batch-adaptive MLMC approaches [27, 71], our AMLMC circumvents the expense of generating meshes on the fly. Furthermore, our application of stochastic meshes is more efficient than the batch-adaptive algorithm for cases without uniform coercivity, like in the lognormal case. Moreover, for cases where the solving cost is higher than the assembly cost, we discuss the use of iterative solvers and compare their efficiency with direct ones. To save computational work, we propose a goal-oriented stopping criterion for the iterative solver.

Theoretically, we characterize those problems where adaptivity provides a noticeable advantage, namely those where the error density blows up in $L^1_P(\mathcal{D} \times \Omega)$, as we refine the mesh around the singularities. We provide a slight generalization of the MLMC complexity theorem, cf. (13), in Theorem 1, thus allowing the MLMC base level to converge to the exact solution, although at a relatively slow rate while essentially preserving the complexity in (13). Corollary 1 further provides an estimate for the computational work of AMLMC by identifying the multiplicative constants in terms of the quasi-norm of problem-dependent error density. The pointwise convergence of the error density as $\text{TOL} \rightarrow 0$, based on proper local averages, is fundamental to delivering theoret-

ical results on stopping, asymptotic accuracy, and efficiency, as proved in [65] and inherited naturally by our AMLMC algorithm. Furthermore, the efficient computation of these local averages in the error estimate is a contribution of this work, improving the results in [65].

Our 2D numerical experiments yield results consistent with the theoretical predictions, namely, (i) the a posteriori error estimates are sharp for bias and variance predictions with singularities and lognormal coefficients present, and (ii) AMLMC exhibits advantages compared to SMLMC, both on its complexity and ability to estimate the errors. More substantial computational gains are expected in higher dimensions.

The outline of this study is as follows: Section 2 presents the problem setting by first describing the boundary value problem under consideration, which is a particular class of elliptic PDEs with random coefficients. Then, the goal-oriented adaptive FEM strategy is introduced and the MLMC method with uniform refinements for estimating the expected values of linear functionals of the random PDE solution is formulated. AMLMC, our goal-oriented adaptive finite element MLMC algorithm, is presented in Section 3. Section 4 presents first the numerical implementation details of AMLMC, then numerical results of applying the AMLMC algorithm to a 2D boundary value problem of an elliptic PDE with a stochastic coefficient field, not bounded away from zero nor bounded from above, and with a geometric singularity at the meeting point between Dirichlet and Neumann boundaries. We observe that, for the same accuracy requirement, our AMLMC requires less work and is more reliable than MLMC on uniform meshes. Finally, Section 5 offers the conclusions.

2. Background material

2.1. Problem setting

We consider the problem of approximating the expected value of a scalar quantity of interest (QoI), which is a function of the solution to (1), a boundary value problem (BVP) for a linear second-order PDE with a stochastic coefficient field. For a given h -adaptive FEM, we will use a sample-based method to approximate the expected value.

2.1.1. BVP for an elliptic PDE with smooth stochastic data

Let $(\Omega, \mathcal{F}, \mathbb{P})$ be a complete probability space and let \mathcal{D} be an open and bounded polygonal/polyhedral domain in \mathbb{R}^d , $d \geq 2$, with boundary $\partial\mathcal{D}$. With homogeneous Dirichlet and Neuman boundary conditions, the BVP with random data is to find $u : \mathcal{D} \times \Omega \rightarrow \mathbb{R}$ that almost surely (a.s.) for $\omega \in \Omega$ solves (1). The model diffusivity coefficient considered here takes the form

$$a(x, \omega) = \exp \left(\sum_{i \geq 0} \xi_i(\omega) \sqrt{\lambda_i} \theta_i(x) \right), \quad x \in \mathcal{D}, \quad (2)$$

where $(\lambda_i)_{i \geq 0}$ is a monotone decreasing sequence of non-negative numbers, $(\theta_i)_{i \geq 0}$ are trigonometric functions in \mathbb{R}^d , and $(\xi_i)_{i \geq 0}$ are i.i.d. $\mathcal{N}(0,1)$ random variables. For the well-posedness and solution regularity for problem (1) with a lognormal coefficient field (2), we refer to [5, 8, 17, 36, 68]. There, well posedness requires control on the pathwise coercivity cf. [5, 89], given by Assumption 1.

Assumption 1 (Well-posedness). *To ensure the well posedness of the solution to (1) in $L_{\mathbb{P}}^k(\Omega; H^1(\mathcal{D}))$ for any $k \geq 1$, we assume that*

- $a_{\min}(\omega) = \min_{\mathbf{x} \in \mathcal{D}} a(\mathbf{x}; \omega) > 0$ a.s. and $1/a_{\min} \in L_{\mathbb{P}}^q(\Omega)$, for all $q \in (0, \infty)$.
- $a \in L_{\mathbb{P}}^q(\Omega, C^1(\overline{\mathcal{D}}))$, for all $q \in (0, \infty)$.
- $f \in L_{\mathbb{P}}^{q^*}(\Omega, L^2(\mathcal{D}))$ for some $q^* > 2$.

Here, $L_{\mathbb{P}}^q(\Omega)$ denotes the space of random variables with finite q -th moment in $(\Omega, \mathcal{F}, \mathbb{P})$. We will later also use the notation $L_{\mathbb{P}}^q(\Omega \times \mathcal{D})$ when the integration is with respect to the product measure of \mathbb{P} and the Lebesgue measure.

Assumption 1 is satisfied by our numerical examples. However, pathwise regularity connects with the p -summability of sufficiently high order derivatives of the auxiliary sum $\sum_{i \geq 0} \sqrt{\lambda_i} \theta_i(x)$. Indeed, the fact that the coefficient function (2) is not uniformly bounded away from 0 makes the analysis more technically challenging. As will be elaborated on later, this feature calls for stochastic mesh selection because $Q(u)$ is unbounded.

The QoI is assumed to be given by a deterministic, real-valued, bounded linear functional Q of the stochastic solution u , and the aim is to approximate its expected value, $\mathbb{E}[Q(u)]$, to a given accuracy TOL and confidence level.

2.1.2. Goal-oriented adaptive FEM

In many engineering applications, the primary goal of a computation is to estimate expected values of functionals of the solution of the BVP. The standard deterministic technique for error estimation, applied pathwise in this work, is the use of a dual weighted error representation, cf. Section 2.1 in [65]. For more on the dual weighted residual (DWR) approach, see, e.g., [3, 10, 13]. The approximation error in a linear functional of the solution is then estimated by

$$|Q(u) - Q(u_{\text{FEM}})| \leq \sum_i |r_i| |z_i|,$$

where u_{FEM} is the FEM approximation of u , the sum is taken over all elements, and r_i and z_i are elementwise contributions from a residual and the corresponding dual solution, respectively. Following the analysis in [65], this study uses an error expansion with computable leading order term, namely,

$$Q(u) - Q(u_{\text{FEM}}) \sim \sum_i \bar{\rho}_i h_i^{p+d},$$

cf. (36). Here, d is the dimension of the domain, and p is the approximation order of the FEM. The primary advantage of this expansion is that the approximate error density $\bar{\rho}_i$, computed using both primal and dual solutions, is essentially independent of the mesh size and the theoretically optimal mesh size can be expressed in terms of the asymptotic error density, ρ , cf. Theorem 2.1 and Corollary 2.2 in [65]. Letting $h(x) : \mathcal{D} \rightarrow \mathbb{R}^+$ be the mesh size function, the error in the output functional can then be approximated as

$$Q(u) - Q(u_{\text{FEM}}) \simeq \int_{\mathcal{D}} \rho(x) h(x)^p dx. \quad (3)$$

Similarly, the computational cost for the assembly and solution steps can be expressed using the mesh function. Thus, a natural step is to formulate a variational problem to choose the optimal mesh function subject to an error budget constraint, see Section 3. This formulation provides a quantitative measure to understand the potential of adaptivity on a given problem and guides the construction of related adaptive algorithms. In this work, the deterministic adaptive algorithm developed in [65] is used pathwise. The pointwise convergence of the error density was proven in [65] where, using ideas from [62–64], it was exploited to show the stopping, accuracy, and efficiency of the deterministic adaptive algorithm. The error density-based goal-oriented adaptive algorithm we employ has a universal nature. Its success in optimal control problems, cf. [50], is an example of this versatility.

Note that this notion of error densities can be extended to nonlinear problems and nonlinear observables, as described in [65, Remark 2.4], and higher-order approximations, [65, Section 2.4].

In what follows, we will use these h -adaptive FEM algorithms to define the AMLMC levels, characterizing them by a sequence of error tolerances following [46, 47]. These error tolerances will control both weak and strong errors. Furthermore, we will focus on examples where locally refined meshes provide an advantage due to geometry induced singularities, a commonplace in engineering applications.

2.1.3. Multilevel Monte Carlo

MLMC uses hierarchical control variates to substantially reduce the computational cost of MC. Thus, it uses a hierarchy of $L + 1$ meshes defined by decreasing mesh sizes, indexed by their levels $\ell = 0, 1, \dots, L$, and the telescopic representation of the expected value of the finest approximation. Thus, letting Q_ℓ denote the approximation of Q on level ℓ ,

$$\mathbb{E}[Q_L] = \mathbb{E}[Q_0] + \sum_{\ell=1}^L \mathbb{E}[Q_\ell - Q_{\ell-1}].$$

Then, the MLMC estimator approximates each expected value in the previous equation by a sample average, namely,

$$\mathcal{A}_{MLMC} = \frac{1}{M_0} \sum_{n=1}^{M_0} Q_0(\omega_{0,n}) + \sum_{\ell=1}^L \frac{1}{M_\ell} \sum_{n=1}^{M_\ell} (Q_\ell(\omega_{\ell,n}) - Q_{\ell-1}(\omega_{\ell,n})), \quad (4)$$

where $\{\omega_{\ell,n}\}_{n=1, \dots, M_\ell}^{\ell=0, \dots, L}$ denote i.i.d. realizations of the mesh-independent random variables. In MLMC, it is fundamental to evaluate both terms in the difference

$$\Delta Q_\ell(\omega_{\ell,n}) = Q_\ell(\omega_{\ell,n}) - Q_{\ell-1}(\omega_{\ell,n}) \quad (5)$$

with the same outcome of $\omega_{\ell,n}$. This implies that $\text{Var}[\Delta Q_\ell] \rightarrow 0$, as $\ell \rightarrow \infty$, provided that the numerical approximation Q_ℓ converges strongly.

To simplify the presentation, introduce the notation

$$V_\ell = \begin{cases} \text{Var}[Q_0], & \ell = 0, \\ \text{Var}[Q_\ell - Q_{\ell-1}], & \ell > 0. \end{cases} \quad (6)$$

The average computational work for generating \mathcal{A}_{MLMC} is

$$W_{MLMC} = \sum_{\ell=0}^L M_\ell W_\ell, \quad (7)$$

where W_ℓ is the average cost of generating ΔQ_ℓ . We build the estimator (4) to approximate $\mathbb{E}[Q]$ with accuracy $\text{TOL} > 0$ with high probability. Therefore, we introduce a splitting parameter $\theta \in (0, 1)$ and enforce

$$\text{Bias Constraint: } |\mathbb{E}[Q] - \mathbb{E}[Q_L]| \leq (1 - \theta)\text{TOL}, \quad (8)$$

$$\text{Statistical Constraint: } \text{Var}[\mathcal{A}_{MLMC}] = \sum_{\ell=0}^L \frac{V_\ell}{M_\ell} \leq \left(\frac{\theta\text{TOL}}{C_\xi} \right)^2, \quad (9)$$

where the parameter $C_\xi > 0$ is chosen depending on the desired confidence level in the error control. Thus, the bias constraint determines $L(\text{TOL})$ whereas the statistical constraint, which is motivated by a central limit theorem approximation, cf. [45], determines the optimal number of samples across levels.

Given L and θ , minimizing the work (7) subject to the constraint (9) and relaxing the integers into real values, leads to the optimal number of samples per level in \mathcal{A}_{MLMC} ,

$$M_\ell = \left(\frac{C_\xi}{\theta\text{TOL}} \right)^2 \sqrt{\frac{V_\ell}{W_\ell}} \sum_{k=0}^L \sqrt{W_k V_k}. \quad (10)$$

Substituting the ceiling of these optimal M_ℓ in the total work (7) yields the upper bound:

$$W_{MLMC} = \left(\frac{C_\xi}{\theta\text{TOL}} \right)^2 \left(\sum_{\ell=0}^L \sqrt{W_\ell V_\ell} \right)^2 + \sum_{\ell=0}^L W_\ell. \quad (11)$$

Under the standard assumptions for MLMC, the first term in the last equation dominates the second one as $\text{TOL} \rightarrow 0$. Thus, since $L(\text{TOL}) \rightarrow \infty$ as $\text{TOL} \rightarrow 0$, the different computational complexity regimes of MLMC are determined by the behavior of $\sum_{\ell=0}^L \sqrt{W_\ell V_\ell}$. Indeed, if $\sum_{\ell=0}^{\infty} \sqrt{W_\ell V_\ell} < \infty$ then the MLMC complexity is TOL^{-2} , while if $W_\ell V_\ell = \mathcal{O}(1)$, then the MLMC complexity is the larger $\text{TOL}^{-2} L^2(\text{TOL})$. Finally, if $W_\ell V_\ell \rightarrow \infty$, the MLMC complexity deteriorates even further. For example, if the product $W_\ell V_\ell$ grows geometrically, the MLMC complexity is dominated by the deepest level, namely, $\text{TOL}^{-2} W_{L(\text{TOL})} V_{L(\text{TOL})}$, which still improves on the corresponding MC complexity.

Following Giles, in the MLMC standard analysis, one usually makes the even more precise assumptions:

Assumption 2. *Assume, for some $\kappa > 1$, a variance convergence rate $V_\ell \lesssim \kappa^{-q_s \ell}$, a bias convergence rate $|\mathbb{E}[Q] - \mathbb{E}[Q_\ell]| \lesssim \kappa^{-q_w \ell}$ and a work per sample $W_\ell \lesssim \kappa^{\gamma \ell}$. Moreover, assume that*

$$q_w \geq \min(q_s, \gamma)/2 > 0. \quad (12)$$

When Assumption 2 is satisfied, the MLMC computational work has, as $\text{TOL} \rightarrow 0$, the asymptotic behavior

$$W_{\text{MLMC}} \lesssim \begin{cases} \text{TOL}^{-2}, & \text{if } q_s > \gamma, \\ \text{TOL}^{-2} (\log \text{TOL}^{-1})^2, & \text{if } q_s = \gamma, \\ \text{TOL}^{-2(1+\frac{\gamma-q_s}{2q_w})}, & \text{if } q_s < \gamma, \end{cases} \quad (13)$$

see e.g. Theorem 3.1 in [33], or Corollaries 2.1 and 2.2 in [39]. Note that (12) is used to ensure that the second term in (11) is asymptotically negligible compared to the first term.

We now state a slightly generalized version of the MLMC complexity theorem allowing the coarsest level to be refined as $\text{TOL} \rightarrow 0$. This is particularly relevant when considering the complexity of adaptive MLMC algorithms because they usually rely on asymptotic properties, which become sharper as the largest element in the discretization is refined to ensure consistent approximation.

Theorem 1 (MLMC Complexity with variable level 0). *Take $0 \leq \epsilon \ll 1$. Let Assumption 2 hold and choose $L(\text{TOL})$ to be the minimum integer that satisfies the bias constraint. If the MLMC base level 0 is such that its average work per sample satisfies*

$$W_0 \lesssim \begin{cases} (\log \text{TOL}^{-1})^\epsilon, & \text{if } q_s > \gamma, \\ (\log \text{TOL}^{-1})^2, & \text{if } q_s = \gamma, \\ \text{TOL}^{-\frac{\gamma-q_s}{q_w}}, & \text{if } q_s < \gamma, \end{cases} \quad (14)$$

the asymptotic MLMC computational work then satisfies

$$W_{\text{MLMC}} \lesssim \begin{cases} \text{TOL}^{-2} (\log \text{TOL}^{-1})^\epsilon, & \text{if } q_s > \gamma, \\ \text{TOL}^{-2} (\log \text{TOL}^{-1})^2, & \text{if } q_s = \gamma, \\ \text{TOL}^{-2(1+\frac{\gamma-q_s}{2q_w})}, & \text{if } q_s < \gamma, \end{cases} \quad (15)$$

cf. (13).

Proof. The proof is a direct consequence of the standard MLMC complexity theorem. It amounts to bounding the relative increase of the MLMC work caused by dropping the first $k(\text{TOL})$ levels, out of $L(\text{TOL})$, given an arbitrary fixed 0-level. Ignoring the second term of (11), which is asymptotically negligible as $\text{TOL} \rightarrow 0$ by Assumption 2, this amounts to bounding the relative increase in $S_L = \sum_{\ell=0}^L \sqrt{V_\ell W_\ell}$. To analyse this increase, choose $L = L(\text{TOL})$ to satisfy the bias constraint, let $\widehat{V}_k = \text{Var}[Q_k] \approx V_0$ be the single level variance, for all $k < L$, and assume for simplicity of notation that the costs of sampling Q_ℓ and ΔQ_ℓ are the same.

The MLMC complexity remains unchanged provided that, for some $K > 0$,

$$\sqrt{\widehat{V}_k W_k} + \sum_{\ell=k+1}^L \sqrt{V_\ell W_\ell} \leq K \sum_{\ell=0}^L \sqrt{V_\ell W_\ell},$$

or equivalently,

$$\sqrt{\widehat{V}_k W_k} \leq (K-1) \sum_{\ell=0}^L \sqrt{V_\ell W_\ell} + \sum_{\ell=0}^k \sqrt{V_\ell W_\ell}. \quad (16)$$

For $q_s \leq \gamma$, when S_L is unbounded as $\text{TOL} \rightarrow 0$, we can satisfy (16) while $k \rightarrow \infty$ as $\text{TOL} \rightarrow 0$ using the following specific choices.

For $q_s < \gamma$, where the summands $\sqrt{V_\ell W_\ell}$ increase with ℓ , choosing $k(\text{TOL})$ such that

$$W_{k(\text{TOL})} \leq \widehat{C}^2 V_{L(\text{TOL})} W_{L(\text{TOL})}$$

satisfies (16) with $K = 1 + \widehat{C} \sqrt{\widehat{V}_k}$. The fact that $V_{L(\text{TOL})} W_{L(\text{TOL})} \rightarrow \infty$ as $\text{TOL} \rightarrow 0$, confirms that it is a feasible to let $k(\text{TOL}) \rightarrow \infty$ as $\text{TOL} \rightarrow 0$.

When $q_s = \gamma$ it holds that $\sum_{\ell=1}^L \sqrt{V_\ell W_\ell} = L \sqrt{V_1 W_1}$ and consequently choosing $k(\text{TOL})$ such that

$$W_{k(\text{TOL})} \leq \left(\widehat{C} L(\text{TOL}) \right)^2$$

satisfies (16) with $K = 1 + \widehat{C} \sqrt{\widehat{V}_k / (V_1 W_1)}$. Since $L(\text{TOL}) \simeq \log(\text{TOL}^{-1})$ we can satisfy the asymptotic bound by letting $W_{k(\text{TOL})} \leq \widehat{C} (\log(\text{TOL}^{-1}))^2$ for some other \widehat{C} .

In the case $q_s > \gamma$, where $S_\infty = \sum_{\ell=0}^\infty \sqrt{V_\ell W_\ell}$ is finite, we need to accept a slightly increased complexity if we let $k \rightarrow \infty$ as $\text{TOL} \rightarrow 0$. To quantify this increase, let $f : \mathbb{R}^+ \mapsto \mathbb{R}^+$ be a strictly increasing, unbounded, function and require that

$$W_{k(\text{TOL})} \leq f(\text{TOL}^{-1}).$$

Since $\sum_{\ell=0}^{L(\text{TOL})} \sqrt{V_\ell W_\ell} \rightarrow S_\infty$ as $\text{TOL} \rightarrow 0$, we can find a constant $K > 1$, depending on both \widehat{V}_k and S_∞ , such that

$$\sqrt{\widehat{V}_k W_k} \leq (K-1) \sqrt{f(\text{TOL}^{-1})} \sum_{\ell=0}^{L(\text{TOL})} \sqrt{V_\ell W_\ell},$$

for all sufficiently small TOL . Assuming further that $\text{TOL} < (f^{-1}(1))^{-1}$, this implies

$$\sqrt{\widehat{V}_k W_k} + \sum_{\ell=k+1}^{L(\text{TOL})} \sqrt{V_\ell W_\ell} \leq K \sqrt{f(\text{TOL}^{-1})} \sum_{\ell=0}^{L(\text{TOL})} \sqrt{V_\ell W_\ell},$$

and consequently the MLMC complexity increases to $\text{TOL}^{-2} f(\text{TOL}^{-1})$, at worst. Choosing $f(x) \propto (\log x)^\epsilon$, $x \in [1, \infty)$, corresponds to the statement of this theorem and completes the proof. \square

Remark 1 (MLMC with deterministic meshes). *When approximating the solution of an RPDE with finite elements on regular triangulations, the parameter $h > 0$ refers to either the maximum element diameter or another characteristic length. Here, because we use quadrilateral isotropic elements, h will be the side length. Denoting the corresponding approximate solution by $u_h(\omega)$ and using piecewise linear or piecewise d -multilinear continuous finite element approximations, and with the previous assumptions, it can be shown [89, Corollary 3.1] that, in the absence of singularities, asymptotically as $h \rightarrow 0$:*

- $|\mathbb{E}[Q(u) - Q(u_h)]| \lesssim Q_W h^2$ for a constant $Q_W > 0$.
- $\text{Var}[Q(u) - Q(u_h)] \lesssim Q_S h^4$ for a constant $Q_S > 0$.

Furthermore, assuming an average cost per sample of the order of $h^{-(d+\gamma)}$, with $1 \leq \gamma \leq 3$, a direct application of Theorem 1 yields the complexity

$$W_{\text{MLMC}} \propto \text{TOL}^{-\max(2, d\gamma/2)} (\log \text{TOL})^{2\chi}$$

with $\chi = 1$ if $d\gamma - 4 = 0$ and $\chi = 0$ elsewhere. The corresponding MC method has the worse complexity

$$W_{\text{MC}} \propto \text{TOL}^{-(2+d\gamma/2)}.$$

Observe that in the presence of singularities, both the weak and strong convergence rates decrease, and SMLMC yields a deteriorated complexity. This will be the case for the examples considered in Section 4.2. There, AMLMC will yield a complexity corresponding to smooth problems, provided the corresponding quasi-norm of the error density remains bounded.

3. Adaptive Multilevel Monte Carlo

For this analysis, we assume that the average work of generating one approximate sample of Q is approximately proportional to the average number of elements N , of the FEM discretization; either because the linear solver is optimal or the assembly cost dominates the cost of the linear solver for the relevant range of tolerances, as in Example 2 in Section 4.

We write the approximation of the expected number of elements as

$$\mathbb{E}[N] = \int_{\mathcal{D}} \mathbb{E}[h^{-d}] \quad (17)$$

where $h : D \times \Omega \rightarrow \mathbb{R}^+$ is a stochastic mesh size function used in the FEM approximation; moreover, we assume that the bias is approximated by the first term in the expansion, cf. (3),

$$\int_{\mathcal{D}} \mathbb{E}[\rho h^p] \quad (18)$$

for a non-negative error density $\rho \in L_{\mathbb{P}}^{\frac{d}{p+d}}(D \times \Omega)$; cf. Theorem 2.1 in [65]. By assuming $\rho \geq 0$, we ignore any cancellation of error contributions at this stage; both [65] and the numerical experiments in Section 4 involve TOL-dependent positive lower and upper bounds on ρ , which we omit here. The bias model (18) is an approximation both in the sense that higher-order terms in the error expansion are omitted and that unattainable continuous h is used. However, it is a useful tool for examining what can be achieved using adaptive mesh refinement and sampling.

First, we will present the optimal, stochastic, continuously varying mesh function $h^* : D \times \Omega \rightarrow \mathbb{R}^+$ as a function of the stochastic error density; i.e., h^* minimizes the expected work required to obtain a given bias. Then we suggest an adaptive MLMC estimator as an approximation to the optimum, which is suitable when a singularity induced by the deterministic geometry is the primary reason to use locally refined meshes.

3.1. Optimal single level mesh distribution for a given bias tolerance

In a single-level MC having a fixed split between bias and statistical errors, different methods differ only via their expected work per sample. Thus, minimizing the expected work per sample, modeled as the expected number of elements (17), subject to the constraint that the bias model (18) equals a prescribed tolerance TOL_{bias} , via a standard Lagrange multiplier technique (Appendix B) leads to the theoretically optimal stochastic mesh size

$$h^*(x; \omega) = \frac{\text{TOL}_{\text{bias}}^{1/p}}{\left(\int_{\mathcal{D}} \mathbb{E} \left[\rho^{\frac{d}{p+d}} \right] \right)^{1/p}} \rho(x; \omega)^{-\frac{1}{p+d}} \quad (19)$$

with an associated optimal mean work per sample proportional to

$$\int_{\mathcal{D}} \mathbb{E}[(h^*)^{-d}] = \frac{\left(\int_{\mathcal{D}} \mathbb{E}\left[\rho^{\frac{d}{p+d}}\right]\right)^{\frac{p+d}{p}}}{\text{TOL}_{\text{bias}}^{d/p}} = \left(\frac{\|\rho\|_{L_{\frac{p}{p+d}}(\mathcal{D} \times \Omega)}}{\text{TOL}_{\text{bias}}}\right)^{d/p}. \quad (20)$$

Thus, the optimal strategy, for single-level MC, does not evenly distribute the error contributions over the samples. Indeed, for this strategy, the leading order error estimate satisfies

$$\int_{\mathcal{D}} \rho(x; \omega) h^*(x; \omega)^p dx = \frac{\text{TOL}_{\text{bias}}}{\int_{\mathcal{D}} \mathbb{E}\left[\rho^{\frac{d}{p+d}}\right]} \int_{\mathcal{D}} \rho(x; \omega)^{\frac{d}{p+d}} dx \quad (21)$$

for each sample. Equation (21) is the motivation for the AMLMC algorithm proposed in this section.

Similarly, minimizing the work model (17) under the same bias constraint using only uniform meshes leads to

$$h_{\text{uni}}^*(\omega) = \text{TOL}_{\text{bias}}^{1/p} \frac{\left(\int_{\mathcal{D}} \rho(x; \omega) dx\right)^{-\frac{1}{p+d}}}{\mathbb{E}\left[\left(\int_{\mathcal{D}} \rho\right)^{\frac{d}{p+d}}\right]^{1/p}}. \quad (22)$$

Thus, the work estimate corresponding to (20) becomes

$$\begin{aligned} \mathbb{E}[(h_{\text{uni}}^*)^{-d}] \int_{\mathcal{D}} 1 dx &= \frac{\mathbb{E}\left[\left(\int_{\mathcal{D}} \rho\right)^{\frac{d}{p+d}}\right]^{\frac{p+d}{p}}}{\text{TOL}_{\text{bias}}^{d/p}} \int_{\mathcal{D}} 1 dx \\ &= \left(\frac{\|\rho\|_{L^1(\mathcal{D})}}{\text{TOL}_{\text{bias}}}\right)^{d/p} \int_{\mathcal{D}} 1 dx, \end{aligned} \quad (23)$$

and the leading order error estimate per sample is given by

$$(h_{\text{uni}}^*(\omega))^p \int_{\mathcal{D}} \rho(x; \omega) dx = \frac{\text{TOL}_{\text{bias}}}{\mathbb{E}\left[\left(\int_{\mathcal{D}} \rho\right)^{\frac{d}{p+d}}\right]} \left(\int_{\mathcal{D}} \rho(x; \omega) dx\right)^{\frac{d}{p+d}}. \quad (24)$$

Suppose, in contrast, the samples are generated using a fixed, deterministic, mesh. The optimal mesh functions are then those obtained using the deterministic theory in [65] with the expected value of the stochastic error density. Here, the optimized work model for deterministic adaptive meshes is given by

$$\int_{\mathcal{D}} (h_{\text{det}}^*(x))^{-d} dx = \left(\frac{\|\rho\|_{L_{\frac{p}{p+d}}(\Omega)}}{\text{TOL}_{\text{bias}}}\right)^{d/p}, \quad (25)$$

while that for deterministic uniform meshes is given by

$$(h_{\text{uni,det}}^*)^{-d} \int_{\mathcal{D}} 1 \, dx = \left(\frac{\|\rho\|_{L_{\mathbb{F}}^1(\mathcal{D} \times \Omega)}}{\text{TOL}_{\text{bias}}} \right)^{d/p} \int_{\mathcal{D}} 1 \, dx. \quad (26)$$

Repeated use of Jensen's inequality confirms that

$$\|\rho\|_{L_{\mathbb{F}}^{\frac{d}{p+d}}(\mathcal{D} \times \Omega)}^{d/p} \leq \left\{ \begin{array}{l} \left\| \|\rho\|_{L^1(\mathcal{D})} \right\|_{L_{\mathbb{F}}^{\frac{d}{p+d}}(\Omega)}^{d/p} \int_{\mathcal{D}} 1 \, dx \\ \left\| \|\rho\|_{L_{\mathbb{F}}^1(\Omega)} \right\|_{L_{\mathbb{F}}^{\frac{d}{p+d}}(\mathcal{D})}^{d/p} \end{array} \right\} \leq \|\rho\|_{L_{\mathbb{F}}^1(\mathcal{D} \times \Omega)}^{d/p} \int_{\mathcal{D}} 1 \, dx. \quad (27)$$

Consequently, these same relations hold between the work estimates in (20), (23), (25), and (26), as is expected given the relative generality of the optimization problems. All four work estimates coincide in the extreme situation when ρ is constant in $\mathcal{D} \times \Omega$. Similarly, for any $\rho \in L_{\mathbb{F}}^1(\mathcal{D} \times \Omega)$, all four complexity estimates will have the same asymptotic rate as $\text{TOL}_{\text{bias}} \rightarrow 0$. This shows that little is gained by going from uniform and deterministic meshes to adaptively refined and/or sample dependent meshes for problems where $\|\rho\|_{L_{\mathbb{F}}^1(\mathcal{D} \times \Omega)}$ is well behaved, that is, it is uniformly bounded over refinement sequences. However, the $L_{\mathbb{F}}^{\frac{d}{p+d}}$ quasi-norms of error densities can remain bounded although the corresponding L^1 norms are unbounded. Canonical examples in the FEM setting for (1) are: (i) deterministically induced singularities in ρ by the geometry, where h -adaptive FEM uses highly local mesh refinements around singularities, or (ii) log-normal coefficient fields, where the stochastic scaling factors multiplying TOL_{bias} in the right hand sides of (21) and (24) vary hugely. In such cases, this simplified complexity analysis does not directly apply, but the complexity can be estimated by introducing a parametric regularization whose effect goes to zero as a suitable power of TOL_{bias} , see Example 4.1 in [65], which is related to Example 0, 1, and 2 in this work.

3.1.1. A fully stochastic adaptive algorithm

This approach is justified if new local mesh refinements are required for each sample; for example: (i) if the error density has a singularity in a random location, or (ii) if the stochastic coefficient field has a short correlation length relative to the domain size. The algorithm can be developed by combining estimates of $\int_{\mathcal{D}} \mathbb{E} \left[\rho^{\frac{d}{p+d}} \right]$ with the deterministic goal-oriented adaptive algorithm, where motivated by (21) the stopping condition for the adaptive refinements is set to

$$\int_{\mathcal{D}} \rho(x; \omega) h(x; \omega)^p \, dx \leq \text{TOL}_{\text{bias}} \frac{\int_{\mathcal{D}} \rho(x; \omega)^{\frac{d}{p+d}} \, dx}{\int_{\mathcal{D}} \mathbb{E} \left[\rho^{\frac{d}{p+d}} \right]} \quad (28)$$

for each sample, ω , using an unsigned error density ρ . Here, the left-hand side is approximated using the error estimate of the adaptive FEM algorithm. The

stochastic scaling factor

$$\frac{\int_{\mathcal{D}} \rho(x; \omega)^{\frac{d}{p+d}} dx}{\int_{\mathcal{D}} \mathbb{E} \left[\rho^{\frac{d}{p+d}} \right]} \quad (29)$$

corresponds to optimally distributed error contributions from different samples. The numerator in this scaling factor is computed as a by-product of computing the error estimate for each sample. The denominator can be estimated using an (ML)MC estimator. With a view toward the AMLMC setting, we observe that this can be iteratively performed in a continuation type algorithm, as described for other MLMC parameters in [22].

Note that the stochastic scaling factor (29) is unbounded for a log-normal coefficient field in (1). A standard approach in MLMC is to simply distribute the error contributions evenly over the samples, i.e. to replace the scaling factor (29) by the deterministic constant 1. That is far from optimal here.

The problem setting targeted by this work is not of a kind where the fully stochastic adaptive algorithm is optimal; at least not when the computational overhead of generating new computational meshes for each sample is taken into account. Because the focus is on situations where (i) a geometry-induced singularity in a deterministic location justifies highly localized mesh refinements, and (ii) the stochastic coefficient field is smooth with long correlation length but high variability, we expect optimal meshes for all samples to be well approximated by meshes selected from a deterministic sequence of adaptively refined meshes, as described in Section 3.3. Therefore, avoiding the computational overhead of mesh generation during the sampling phase leads to substantial computational gains.

3.2. Multilevel hierarchies of optimal meshes

We consider MLMC estimators obtained by introducing a decreasing sequence of bias tolerances,

$$\text{TOL}_\ell = C^\ell \text{TOL}_0, \quad \ell = 0, 1, \dots, \quad (30)$$

for a given separation constant, $0 < C < 1$, using the optimal single level approximations above. This choice fixes three parameters in Assumption 2: $\kappa = C^{-1}$, $\gamma = d/p$, and $q_w = 1$. (Observe that defining the levels by decreasing tolerances makes q_w independent of the FEM order, p .) The MLMC complexity (13) fundamentally depends on the fourth parameter, q_s , which we now turn to.

Here, we consider only smooth stochastic coefficient fields, whose pathwise regularity allows us to use the error expansion from [65] to obtain $q_s = 2q_w = 2$. However, problems with rough coefficients require a different approach to the one considered here; see for instance [40] for the case of uniform discretizations.

Now we want to estimate the multiplicative constants in our models of the work and the strong convergence in terms of (quasi-) norms of the error density.

Any family of mesh size functions parametrized by TOL_ℓ on the form

$$h_\ell(x; \omega) = \text{TOL}_\ell^{1/p} f(x; \omega), \quad (31)$$

such as the optimal meshes in (19) and (22) with $\text{TOL}_{\text{bias}} = \text{TOL}_\ell$, satisfies

$$\begin{aligned} Q_\ell(\omega) - Q_{\ell-1}(\omega) &\simeq \int_{\mathcal{D}} \rho(x; \omega) (h_{\ell-1}(x; \omega)^p - h_\ell(x; \omega)^p) dx \\ &= \text{TOL}_\ell (C^{-1} - 1) \underbrace{\int_{\mathcal{D}} \rho(x; \omega) f^p(x; \omega) dx}_{K_1(\omega)} \end{aligned}$$

and

$$\int_{\mathcal{D}} h_\ell^{-d}(x; \omega) dx \simeq \text{TOL}_\ell^{-d/p} \underbrace{\int_{\mathcal{D}} f^{-d}(x; \omega) dx}_{K_2(\omega)},$$

such that

$$\text{Var}[Q_\ell - Q_{\ell-1}] \simeq \text{TOL}_\ell^2 (C^{-1} - 1)^2 \text{Var}[K_1] \quad (32)$$

and

$$\int_{\mathcal{D}} \mathbb{E}[h_\ell^{-d}] + \int_{\mathcal{D}} \mathbb{E}[h_{\ell-1}^{-d}] \simeq \text{TOL}_\ell^{-d/p} (1 + C^{d/p}) \mathbb{E}[K_2]. \quad (33)$$

Consequently, as long as $\text{Var}[K_1]$ and $\mathbb{E}[K_2]$ are bounded, Assumption 2 is satisfied with $\kappa = C^{-1}$, $\gamma = d/p$, $q_s = 2$, and $q_w = 1$.

We can estimate the problem-dependent multiplicative constants in the complexities, by letting V_ℓ and W_ℓ be given by (32) and (33), respectively, in the summands with $\ell \geq 1$ in the sum $\sum_{\ell=0}^L \sqrt{W_\ell V_\ell}$, which appears in the asymptotically dominant first term of the MLMC work model (11). Then

$$\begin{aligned} V_\ell W_\ell &= \text{Var}[Q_\ell - Q_{\ell-1}] \left(\int_{\mathcal{D}} \mathbb{E}[h_\ell^{-d}] + \int_{\mathcal{D}} \mathbb{E}[h_{\ell-1}^{-d}] \right) \\ &\simeq \text{TOL}_0^{2-d/p} (C^{-1} - 1)^2 (1 + C^{d/p}) \text{Var}[K_1] \mathbb{E}[K_2] C^{(2-d/p)\ell}, \quad \ell \geq 1. \end{aligned}$$

Summing $\sqrt{V_\ell W_\ell}$ over $\ell = 1, \dots, L$, considering the three cases $d < 2p$, $d = 2p$, and $d > 2p$ for the geometric sum $\sum_{\ell=1}^L C^{(1-\frac{d}{2p})\ell}$, and letting $\text{TOL} \rightarrow 0$ leads to the statement below on the AMLMC complexity. The statement in the corollary uses that for the two cases in (21) and (24)

$$\text{Var}[K_1] = \frac{\text{Var}[Y]}{\mathbb{E}[Y]^2} = (c_V(Y))^2,$$

where $c_V(Y)$ denotes the coefficient of variation of Y , and with $Y = \|\rho\|_{L^{\frac{d}{p+d}}(\mathcal{D})}^{\frac{d}{p+d}}$

and $Y = \|\rho\|_{L^1(\mathcal{D})}^{\frac{d}{p+d}}$, respectively, for the two cases.

Corollary 1 (Adaptive MLMC Complexity). *Assume the work and bias models (17) and (18) hold and the sampling error control satisfies either*

- (i) (21), for finite $\|\rho\|_{L^{\frac{d}{p+d}}(\mathcal{D} \times \Omega)}$, (fully adaptive case), or
- (ii) (24), for finite $\|\|\rho\|_{L^1(\mathcal{D})}\|_{L^{\frac{d}{p+d}}(\Omega)}$, (adaptive selection of uniform meshes).

Then, the MLMC computational work model (7) with M_ℓ given by (10) and $L \in \mathbb{R}^+$ implied by (8) and (30) satisfies

$$W_{\text{MLMC}} \simeq \begin{cases} KTOL^{-2}, & \text{if } d < 2p, \\ KTOL^{-2} (\log TOL^{-1})^2, & \text{if } d = 2p, \\ KTOL^{-d/p}, & \text{if } d > 2p, \end{cases} \quad (34)$$

with $K = K(\rho; C, \text{TOL}_0, \theta, C_\xi) = K_3(\rho)K_4(C, \text{TOL}_0, \theta)K_5(C, \theta, C_\xi)$ for

$$\begin{aligned} K_3 &= \mathbb{E}[K_2] \text{Var}[K_1] \\ &= \begin{cases} \|\rho\|_{L^{\frac{d}{p+d}}(\mathcal{D} \times \Omega)}^{d/p} \left(\text{cv} \left(\|\rho\|_{L^{\frac{d}{p+d}}(\mathcal{D})} \right) \right)^2, & \text{case (i),} \\ \int_{\mathcal{D}} 1 \, dx \|\|\rho\|_{L^1(\mathcal{D})}\|_{L^{\frac{d}{p+d}}(\Omega)}^{d/p} \left(\text{cv} \left(\|\rho\|_{L^1(\mathcal{D})} \right) \right)^2, & \text{case (ii),} \end{cases} \\ K_4 &= \begin{cases} \text{TOL}_0^{-\frac{d}{p}} \left(\sqrt{\frac{V_0}{\text{Var}[K_1]}} \frac{1}{(C^{-1}-1)\sqrt{1+C^{d/p}}} + \text{TOL}_0 \frac{C^{1-\frac{d}{2p}}}{1-C^{1-\frac{d}{2p}}} \right)^2, & \text{if } d < 2p, \\ (\log C)^{-2}, & \text{if } d = 2p, \\ (1-\theta)^{(2-\frac{d}{p})} \left(1 - C^{\frac{d}{2p}-1}\right)^{-2}, & \text{if } d > 2p, \end{cases} \end{aligned}$$

and

$$K_5 = \left(\frac{C_\xi}{\theta} \right)^2 (C^{-1} - 1)^2 (1 + C^{d/p}).$$

The proof is given in Appendix C.

Remark 2 (On integer constraints on L). *The simplification of allowing non-integer values of L in Corollary 1 does not affect the result for $d < 2p$ and $d = 2p$. When $d > 2p$, imposing $L = \lceil L^* \rceil$, where $L^* \in \mathbb{R}^+$ is the value implied by (8) and (30), leads to*

$$K \leq \liminf_{\text{TOL} \rightarrow 0^+} \frac{W_{\text{MLMC}}}{\text{TOL}^{-d/p}} \leq \limsup_{\text{TOL} \rightarrow 0^+} \frac{W_{\text{MLMC}}}{\text{TOL}^{-d/p}} \leq KC^{1-\frac{d}{2p}},$$

with K defined in the corollary.

Remark 3 (On the use of the leading order approximation of bias). *Corollary 1 is stated under the explicit assumption that the bias model (18) holds, and it is used on all levels TOL_ℓ , $\ell = 0, 1, \dots, L$. This model, however, is only the leading order term of the bias as $\text{TOL}_\ell \rightarrow 0$. Theorem 1 allows for letting $\text{TOL}_0 \rightarrow 0$, slowly, as $\text{TOL} \rightarrow 0$, which strengthens the connection to the asymptotic theory. Doing this comes at the cost of a logarithmic factor in the complexity estimate when $d < 2p$, but not when $d \geq 2p$.*

A sharper analysis, relaxing (18) and taking the effect of the non-asymptotic levels in the complexity estimate into account, can be developed for this setting closely following the analysis in [47]. We do not do it here for the sake of length of exposition.

Remark 4 (On the effect of C). *In practical computations, it is unrealistic to assume that $\text{Var}[Q_\ell - Q_{\ell-1}] \rightarrow 0$ as $C \rightarrow 1$. The model (32), with the factor $(C^{-1} - 1)$ is relevant when C is far from 1; we use $C = 1/4$ in the numerical experiments in Section 4. For optimization of C , we can instead use the bound $\text{Var}[Q_\ell - Q_{\ell-1}] \leq 2\text{Var}[Q - Q_\ell] + 2\text{Var}[Q - Q_{\ell-1}]$, which leads to replacing $(C^{-1} - 1)$ by $2(C^2 + 1)$. This can be seen as a penalization on closely spaced tolerances.*

Remark 5 (On the effect of TOL_0). *When $d \geq 2p$, the choice of TOL_0 does not have any effect on the asymptotic estimates in Corollary 1, as long as the choice is fixed with respect to TOL . However, when $d < 2p$ the choice of TOL_0 matters even asymptotically as $\text{TOL} \rightarrow 0$. The factor $K_4(C, \text{TOL}_0, \theta)$ allows for an explicit minimization with respect to TOL_0 to identify the unique minimizer in $(0, \infty)$.*

The constants in the corollary above were obtained under idealized assumptions, some of which were expanded upon in Remarks 2, 3, and 4. Considering these reservations, our particular numerical experiments in Section 4 show good agreement between the modeled and experimentally observed values of V_ℓ (Table 4).

Remark 6 (Dirichlet–Neumann boundary singularity (Needle problem)). *The gains of AMLMC with respect to SMLMC are dimensional dependent. To understand the potential advantages of AMLMC with respect to SMLMC, consider the problem described in Section 4.2. This problem can be generalized to higher dimensions. For instance, to obtain the corresponding formulation in dimension $d = 3$, one uses a 3D cylindrical domain generated by rotating the 2D domain depicted in Figure 1.a around its top boundary. In that case, the Neumann boundary condition is dropped, while the Dirichlet boundary condition corresponding to the axis of rotation, the line segment joining $(0, 0)$ with $(1, 0)$, is maintained, thus yielding the penetrating needle shape. In this problem, all boundary conditions are zero Dirichlet. By its construction, this problem inherits the same singularity as the 2D problem and now the relevant distance to the singularity is the distance to the needle tip. Here, one can argue that the error density quasi-norm is uniformly bounded and for AMLMC we have the full*

FEM order $p = 2$. Thus $d < 2p$ so that, assuming we use an optimal solver, the AMLMC yields TOL^{-2} complexity while the SMLMC yields the worse TOL^{-3} complexity in that case. The situation is even more favorable in $d = 4$, where AMLMC and SMLMC yield $\text{TOL}^{-2} \log^2(\text{TOL}^{-1})$ and TOL^{-4} , respectively.

3.3. A Multilevel Monte Carlo estimator tailored to deterministic adaptivity

In this section we demonstrated that AMLMC, guided by an error density ρ , can provide substantial computational gain compared with the standard MLMC on uniform discretizations, particularly for problems where the norm $\|\rho\|_{L^1_{\mathbb{P}}(\mathcal{D} \times \Omega)}$ is not uniformly bounded over refinement sequences, while $\|\rho\|_{L^{\frac{d}{p+d}}_{\mathbb{P}}(\mathcal{D} \times \Omega)}$ or $\|\|\rho\|_{L^1(\mathcal{D})}\|_{L^{\frac{d}{p+d}}_{\mathbb{P}}(\Omega)}$ do remain uniformly bounded; see case (i) and (ii) in Corollary 1.

For problems where highly localized adaptive mesh refinements are justified by deterministic effects, such as the needle problem with a lognormal coefficient field, we propose an approximation to the fully adaptive case (i) using adaptive selection of graded meshes, generated by the h -adaptive FEM algorithm applied to a deterministic error density, for example the error density obtained when the random coefficient field is replaced by its expected value. Then we use (21) to select the appropriate deterministic mesh for each outcome.

3.3.1. Stochastic acceptance of deterministically generated meshes

The idea in its single-level form is to divide the algorithm into two parts:

- (1) Using a decreasing sequence of tolerances, $\text{TOL}_{\text{det},k} = C_1^k \text{TOL}_{\text{det},0}$ for some $C_1 \in (0, 1)$, we generate FEM discretizations with mesh size functions $h_k : \mathcal{D} \rightarrow \mathbb{R}$, $k = 0, 1, \dots$, using the goal-oriented FEM algorithm applied to the deterministic problem with *unsigned* approximations to the error density.
- (2) Given a bias tolerance, TOL_{bias} , and an estimate $R \approx \int_{\mathcal{D}} \mathbb{E} \left[\rho^{\frac{d}{p+d}} \right]$, we generate approximate samples of Q by starting on the coarsest level, $k = 0$, computing the primal and dual solutions using mesh h_k and the corresponding approximate *signed* error density $\tilde{\rho}_k(x; \omega)$. Repeat for increasing k until

$$\left| \int_{\mathcal{D}} \tilde{\rho}_k(x; \omega) h_k(x)^p dx \right| \leq \frac{\text{TOL}_{\text{bias}}}{R} \left| \int_{\mathcal{D}} \tilde{\rho}_k(x; \omega)^{\frac{d}{p+d}} dx \right|. \quad (35)$$

The MLMC version, defined as before by a sequence (possibly distinct from $\text{TOL}_{\text{det},k}$) of tolerances $\text{TOL}_{\ell} = C^{\ell} \text{TOL}_0$, generates sample pairs $(Q_{\ell}, Q_{\ell-1})$ by applying the procedure in part (2) to the bias tolerances $(\text{TOL}_{\ell}, \text{TOL}_{\ell-1})$.

Note that the goal-oriented FEM algorithm only has to be called once for each mesh h_k , which is then saved for all future samples. This sequence of meshes can be accessed on demand by generating additional refined meshes only when (35) fails to hold for all previously generated meshes. Therefore, in practice parts (1) and (2) interlace.

This approach is particularly useful in the lognormal case, cf. Section 4.3, where we must use a stochastic mesh to efficiently address the lack of uniform coercivity.

4. Implementation and numerical examples

This section presents the algorithms and their implementation for SMLMC and AMLMC; moreover, it shows a numerical comparison between them for elliptic problems with random coefficients. Here, we consider both lognormal constant and a spatially-correlated lognormal fields (Section 4.3.2 and Section 4.3.3), in a 2D physical domain with a geometrically driven singularity.

4.1. Implementation

First, we present the implementation of the numerical approximation of the elliptic problem for a fixed realization of the random coefficient field, followed by SMLMC and AMLMC algorithms and their implementation.

The numerical experiments are written in C++ and run on a workstation with a 2.10GHz Intel Xeon Gold 6230R CPU and 252 GByte RAM. The computational work is measured in FLOPS using the performance application programming interface (PAPI), Version 6.0.0 [90]. The FEM implementation uses the deal.II Library, Version 9.2 [4].

Compute the Primal and Dual Solution The primal and dual solutions u and φ , respectively, to problem (1) are computed on the same quadrilateral mesh (possibly with hanging nodes, handled by the deal.II library [4]), using the same first-order bilinear quadrilateral finite element class Q_1 , see [48], for instance.

The Iterative Solver Control The primal and dual solutions obtained by an iterative solver are denoted by u_{iter} and φ_{iter} , respectively. The algorithm iteratively proceeds, thus simultaneously advancing the pair of primal solvers and dual solvers in each iteration step, checking against the solver stopping tolerance, see Algorithm 1. For each sample, we select the iterative solver tolerance TOL_{iter} to be $\frac{1}{10}$ of the stopping tolerance such that the iterative solver error does not dominate the error. More details can be seen in Algorithm 3, where we use iterative solvers to compute samples in AMLMC. Here, the preconditioned conjugate gradient method is chosen as our iterative solver.

Compute the Error Density The error density ρ is computed using the finite element solutions u_h and φ_h . An approximation of the error density, on a quadrilateral cell K , $\tilde{\rho}_K$, is derived in [65] and written as

$$\tilde{\rho}_K := \frac{1}{48} \sum_{j=1}^4 (a_{11}^* \overline{D_1^2 u_h} \overline{D_1^2 \varphi_h} + a_{22}^* \overline{D_2^2 u_h} \overline{D_2^2 \varphi_h})(x_j^K), \quad (36)$$

where $j = 1, 2, 3, 4$ are the four vertices of the cell K , $D_1^2 u_h$ is the second-order difference quotient over the reference direction x_1 and the notation $\overline{D_1^2 w}$ means the averaged difference quotient $D_1^2 w$. This averaging is required to make the difference quotient uniformly converge to the corresponding derivatives. For discussions on its motivation and fast computation, we refer to Remark 2.1 and Section 2.3 of [65]. From our implemented

data structure (see Algorithm 4), the complexities of computing difference quotients and error densities are provided in Table 1, which improved on the complexities in [65].

We adopted the strategy proposed in [65], which uses a lower bound for the error density, i.e.

$$\bar{\rho} = \text{sgn}(\tilde{\rho}) \max\{|\tilde{\rho}|, \delta\} \quad (37)$$

where $\text{sgn}(\cdot)$ is the sign function, $|\tilde{\rho}|$ is the unsigned computed error density from (37), and $\delta = \frac{\|\tilde{\rho}\|_{L^{\frac{1}{2}}(\mathcal{D})}}{(f_{\mathcal{D}} dx)^2} \sqrt{\text{TOL}}$, with TOL being the tolerance used when generating the meshes (refer to Algorithm 2). The lower bound ensures that the maximum element size asymptotically converges to 0, and the ratio of the error density at two consecutive refinement levels is close to 1 [65]. Because the adaptive algorithm does not include a coarsening step, we impose a TOL-dependent upper bound on the approximate error density to prevent over-refinement because of poor estimates on coarse meshes, cf. [65].

The `deal.II` library uses a tree structure to represent finite element meshes. To efficiently compute the difference quotients and subsequent error densities and error estimates, we implemented Algorithm 4, which extracts horizontal and vertical lines structures from a tree structure.

SMLMC and AMLMC SMLMC uses sequentially refined uniform meshes on the levels and uses a direct solver UMFPACK [24] for linear systems. AMLMC comprises two phases. In phase I, an adaptive mesh hierarchy is generated (Algorithm 2). In phase II, the MLMC sampling is performed on such meshes, to compute the MLMC estimate (4). The same parameters θ and C_{ξ} are used in all AMLMC and SMLMC computations, with $\theta = 0.5$ and $C_{\xi} = 1.96$.

Next, a sample $(Q_{\ell} - Q_{\ell-1})(\omega)$ is generated using Algorithm 3, and the direct solver UMFPACK is applied in the coarsest mesh in AMLMC. The quantity $\mathbb{E} \left[\rho^{\frac{d}{p+d}} \right]$ in (35) is roughly approximated using the coarsest mesh in the hierarchy (Figure 2). Note that this estimate can be improved using an MLMC estimator.

The complexities of the aforementioned implementation methods are summarized in Table 1.

4.2. Example problems

We solve BVP (1) on the domain $\mathcal{D} = [-1, 1] \times [-1, 0] \subset \mathbb{R}^2$ (see Figure 1a), with $\partial\mathcal{D}_1 = \partial\mathcal{D} - \partial\mathcal{D}_2$ and $\partial\mathcal{D}_2 = [-1, 0] \times (0)$, for $f \equiv 1000$. Studies on the effect of the singularity because of the geometry on the Laplace solution regularity [7, 38, 49, 56, 88, 88, 92] show that the regularity of the solution u reduces to $H^{\frac{3}{2}-\epsilon}(\mathcal{D})$ for $\epsilon > 0$, and the pointwise finite element approximation

	Complexity
Assembly	$\mathcal{O}(N^2)$
Direct Solver	$\mathcal{O}(N^3)$
Iterative Solver	$\mathcal{O}(I_{\text{iter}}N)$
Assemble Line(Uniform)	$\mathcal{O}(N \log N)$
Difference Quotient(Uniform)	$\mathcal{O}(N)$
Error Estimation (Uniform)	$\mathcal{O}(N \log^2 \sqrt{N})$
Assemble Line(Adaptive)	$\mathcal{O}(N^2)$
Difference Quotient(Adaptive)	$\mathcal{O}(N)$
Error Estimation (Adaptive)	$\mathcal{O}(N \log^2 N)$

Table 1: Numerical complexities of each simulation part. Note that the complexity for the iterative solver depends on the number of iterations, I_{iter} . The algorithm for the Assemble Line is Algorithm 4. The provided complexity for the adaptive mesh is considered for the worst-case scenario. The difference quotient and error estimation follows a natural implementation in the data structure created by Algorithm 4.

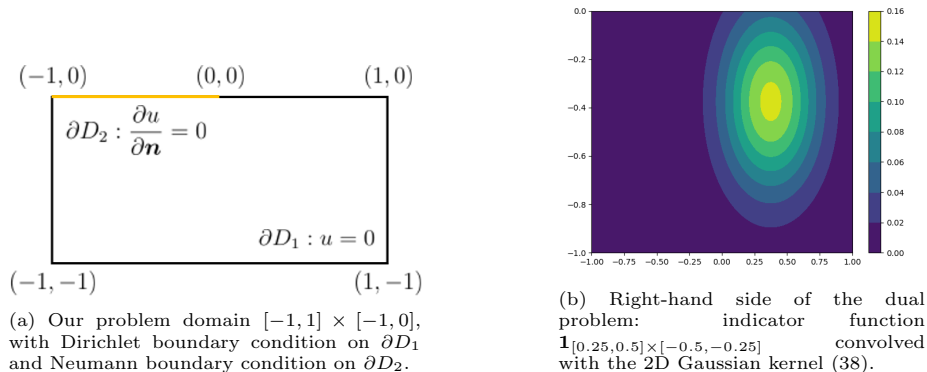


Figure 1: The figure presents: (a) The problem domain and boundary conditions, and (b), a plot of the dual problem right-hand side function.

error for uniform meshes cannot be better than $\mathcal{O}(C(\omega)hr^{\frac{1}{2}})$, where r is the distance to the origin, where the singularity occurs.

In this example, the QoI is the weighted average $Q(u) = (g * \mathbf{1}_{D_0}, u)$, where $*$ is the convolution operator, $\mathcal{D}_0 = [0.25, 0.5] \times [-0.5, -0.25] \subset \mathcal{D}$, and $g(\cdot)$ is the Gaussian density in \mathbb{R}^2 given by

$$g(x) = \frac{1}{\sqrt{(2\pi)^2|\Sigma|}} \exp\left(-\frac{1}{2}(x - \mu)^T \Sigma^{-1}(x - \mu)\right) \quad (38)$$

with mean $\mu = 0$ and covariance $\Sigma = \frac{1}{16}\mathbf{I}$. The corresponding dual problem is (1), with $f = \mathbf{1}_{D_0} * g$.

Figure 1b gives a visualization of the right-hand side of the dual problem. The different numerical examples below differ in the choice of diffusivity coefficient, a .

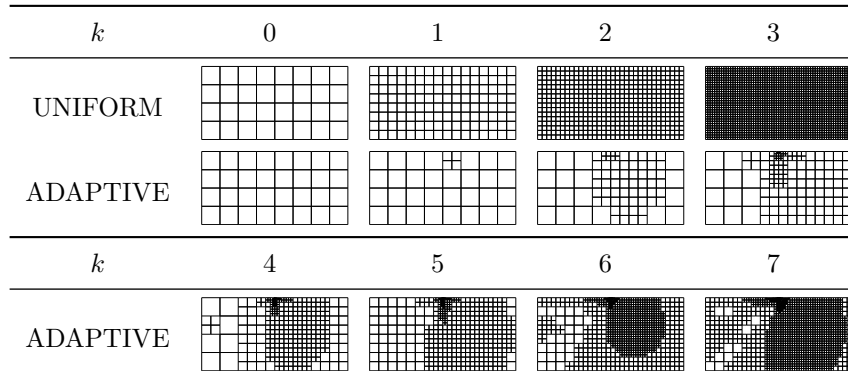


Figure 2: Example 0: The uniform and adaptive mesh hierarchies. Both mesh hierarchies start from the same mesh level 0. As expected, the adaptive meshes are refined towards the singularity from the boundary conditions at $(0, 0)$ and the region most affecting the QoI. The adaptive meshes are generated using Algorithm 2 with $\text{TOL}_k = 2^{-(k+5)}$ and the remaining the parameters mentioned in Section 4.3.1.

4.3. Numerical results

4.3.1. Example 0

Here, we treat problem (1) with a deterministic, constant coefficient $a \equiv \exp(2)$. We consider the problem for uniform and adaptive meshes. The sequence of uniform meshes are globally refined once in each direction per time. The hierarchy of adaptive meshes is generated using Algorithm 2 with the sequence of TOLs being $\text{TOL}_k = 2^{-(k+5)}$, $k = 0, 1, \dots$, at $C_R = 2.5$, $C_S = 3$, and $c = 2$. Figure 2 shows the generated uniform and adaptive meshes.

Figure 3 shows the decay of the error estimate against the number of DoF ($\#\text{DoF}$) for uniform and adaptive mesh hierarchies. The observed convergence rate of the error estimate using adaptive meshes is twice the rate obtained with uniform meshes. Adaptively refined meshes are more resolved around the singularity and the region most affecting the QoI, thus distributing the error contributions more equally over the cells.

Figure 4 plots the $L^1(\mathcal{D})$ norm and $L^{\frac{1}{2}}(\mathcal{D})$ quasi-norm of the error density ρ against the size of the smallest element h_s for uniform and adaptive meshes. The $L^{\frac{1}{2}}(\mathcal{D})$ quasi-norm is defined by

$$\|\rho\|_{L^{\frac{1}{2}}(\mathcal{D})} = \left(\int_{\mathcal{D}} \rho^{\frac{1}{2}} \right)^2. \quad (39)$$

Because of the slit singularity, the smallest element is the one at the origin $(0, 0)$. The growth of $\|\rho\|_{L^1(\mathcal{D})}$ with slope 1 and the constant $\|\rho\|_{L^{\frac{1}{2}}(\mathcal{D})}$ matches the Sobolev regularity $u, \varphi \in H^{\frac{3}{2}-\epsilon}(\mathcal{D})$, for $\epsilon > 0$, see [88].

The asymptotic growth behavior of $\|\rho\|_{L^1(\mathcal{D})}$ for adaptive meshes starts occurs at about the same value of the smallest mesh size, h_s , value as uniform ones (Figure 4). With comparable $\#\text{DoF}$, adaptive meshes have considerably

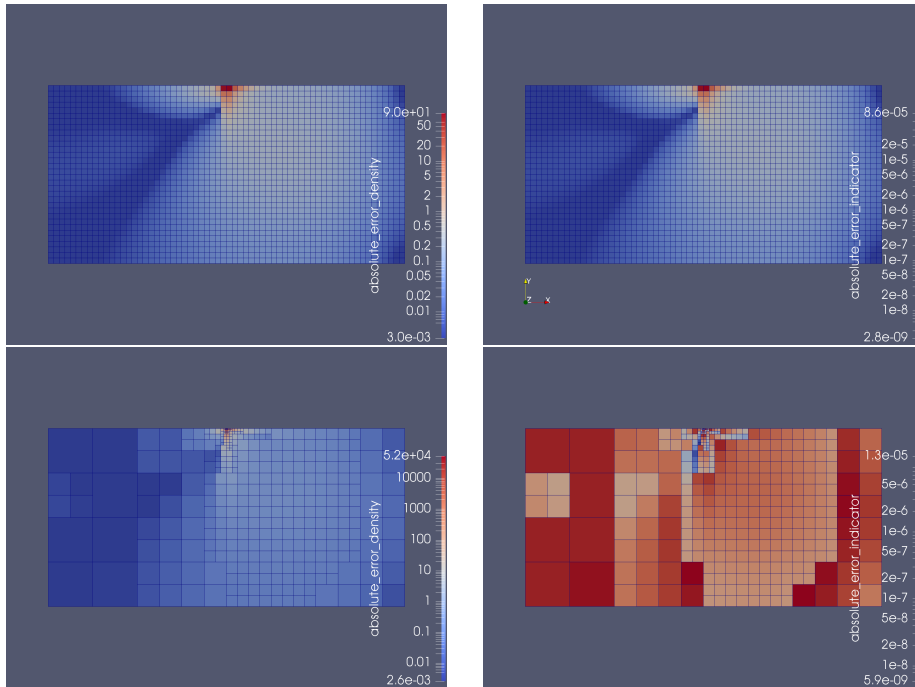
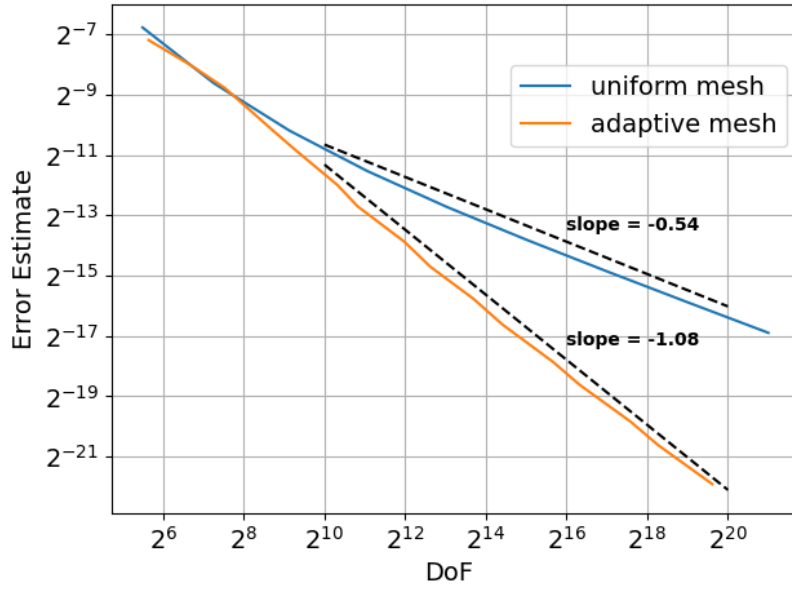


Figure 3: Example 0: The absolute error estimates $e_{est, err}$ (A.3), absolute error densities $|\bar{\rho}|$ from (37), and absolute error indicators $|\tau|$ from (A.1) against #DoF for the uniform and adaptive mesh hierarchies (Figure 2). Top: The convergence of the error estimate against #DoF for uniform and adaptive meshes. Middle: The error density (left) and the absolute error indicator (right) for one uniform mesh. Bottom: The absolute error density (left) and absolute error indicator (right) for one adaptive mesh.

smaller h_s than uniform meshes. They more efficiently capture the singularity than the uniform ones, thereby providing more reliable error estimates. Observe that the numerical results for Example 1, which considers a lognormal constant field a , represent this example as well. When the coefficient a is constant over the domain \mathcal{D} , the QoI (i.e., a linear functional of u) scales linearly with $1/a$, as seen in

$$-\nabla \cdot (\nabla u(\mathbf{x}; \omega)) = \frac{f(\mathbf{x})}{a(\omega)} \text{ for } \mathbf{x} \in \mathcal{D}.$$

Therefore, we postpone the comparison between error and tolerances to Section 4.3.2.

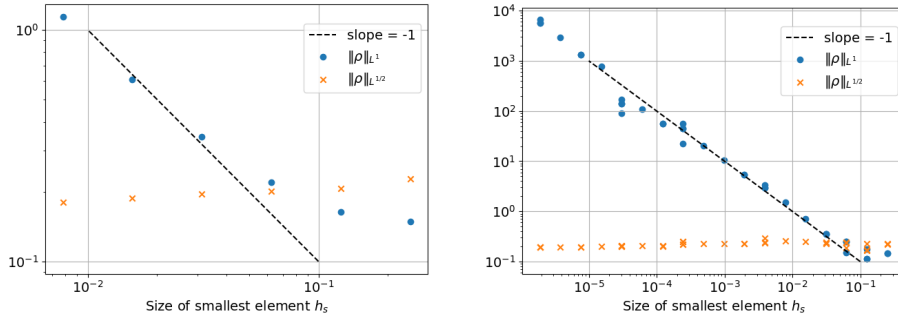


Figure 4: Example 0: Graphs of $L^1(\mathcal{D})$ norm and $L^{\frac{1}{2}}(\mathcal{D})$ quasi-norms of the error density ρ against the size of smallest element h_s on the uniform (left) and adaptive meshes (right) 2. $\|\rho\|_{L^1(\mathcal{D})}$ grows proportional to h_s^{-1} , while $\|\rho\|_{L^{\frac{1}{2}}(\mathcal{D})}$ remains unchanging throughout the meshes. The finest uniform and adaptive meshes in this plot have 33,153 and 13,061 DoF, respectively.

4.3.2. Example 1

In this section, we consider the lognormal constant coefficient field

$$a(x) \equiv \exp(Y), \quad x \in D, \quad (40)$$

where Y is a Gaussian random variable with mean 0 and variance σ^2 .

Figure 5 shows the error estimates against the computational errors in Q_ℓ for SMLMC and AMLMC. The errors are computed by comparing with a reference solution obtained on a refined adaptive mesh with 801,430 DoF.

In SMLMC (left plot of Figure 5), all the samples in one level are obtained from the same mesh. Observe that each level forms a line pattern, and these line patterns share the same slope but are at an offset from each other. It follows that on the same mesh, the error estimate is different from the error (in Q_ℓ) by a constant factor, which is independent of the random sample. As we increase the levels, the error estimates stagnate at an offset below the dashed line, exposing that the uniform meshes underestimate the errors.

In AMLMC case (right plot of Figure 5), one level contains the samples that satisfy a given criterion (refer to Algorithm 3) and are distributed into a range

of (adaptive) auxiliary meshes. Several line patterns having the same slope but different offsets can also be observed, with each line consisting of samples of the same mesh but belonging to different levels. Because of the variation of the stochastic coefficient, computing to a given accuracy incurs a higher cost for certain samples than for others. The magnified views demonstrate that the proposed stochastic mesh selection makes the error contribution smaller where it is inexpensive to do so and larger where it is more expensive to reduce the error. The contrast between cheap and expensive samples follows from using our sample-dependent stopping scheme in AMLMC. The error estimates were slightly overestimated in the last level of the shown adaptive meshes.

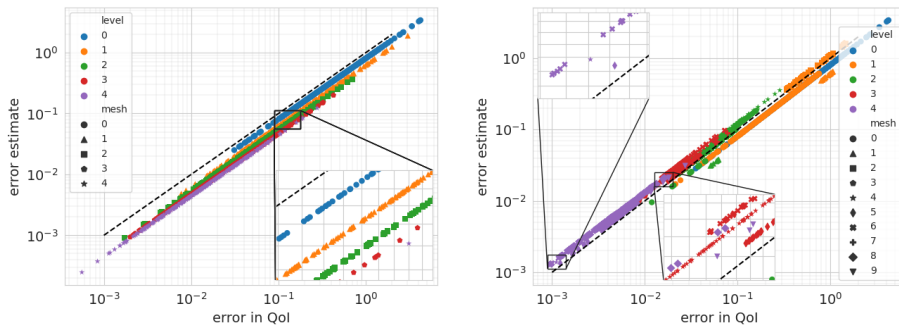


Figure 5: Example 1 with $\sigma^2 = 1$: Errors in QoI (compared to a reference solution) versus error estimates of Q_ℓ for SMLMC (left) and AMLMC (right) for their first 5 levels respectively. The dashed line denotes where the error estimate of Q_ℓ equals the error in Q_ℓ . The dots are samples with colors representing at which MLMC level they belong to, whereas symbols were used to distinguish between auxiliary mesh levels. Observe that $\#\text{DoF}$ grew with the index of the symbols.

In Examples 1 and 2, we fixed a geometric sequence $(\text{TOL}_\ell)_{\ell \geq 0}$, with TOL_0 of AMLMC selected from (2.5) in [34]. In Example 1, the TOL_ℓ used for $\sigma^2 = 1$ and $\sigma^2 = 4$ are $\text{TOL}_\ell = 2 \cdot 4^{-\ell}$ and $\text{TOL}_\ell = 4^{1-\ell}$, respectively.

Figures 6 and 7 show the convergence of mean $E_\ell = |\mathbb{E}(Q_\ell - Q_{\ell-1})|$ and variance V_ℓ and the growth of W_ℓ for SMLMC and AMLMC in Example 1 with $\sigma^2 = 1$. The mean E_ℓ and variance V_ℓ of telescopic differences of AMLMC converge twice faster than the ones of SMLMC with respect to ℓ ; however, the work W_ℓ remains essentially the same. Note that in our setting, the sequence of TOLs in AMLMC decays with a factor of $1/4$, controlling the decay of the sharp error estimate of each sample. From Figure 3, the convergence rate of the error estimate for a fixed realization of the coefficient a on adaptive meshes is proportional to the growth in $\#\text{DoF}$, which is twice the rate of the uniform meshes. Thus, with the level increments, the estimated weak error in AMLMC should decay by a factor of 4; however, the cost increases by a factor of 4, which is the same cost required to globally refine a uniform mesh. In both schemes, the assembly cost is the dominating cost in the coarser levels, and is surpassed by the solver cost as we go deeper on the level ℓ .

Figures 8 and 9 show the convergence of mean E_ℓ and variance V_ℓ and the

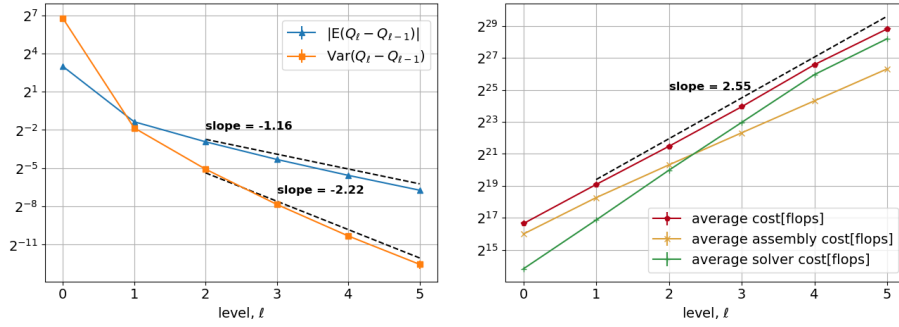


Figure 6: Example 1 with $\sigma^2 = 1$ using SMLMC. Left: Mean and variance of $Q_\ell - Q_{\ell-1}$ for level ℓ , with a 95% confidence interval. Right: The average work per sample (measured in flops) for level ℓ .

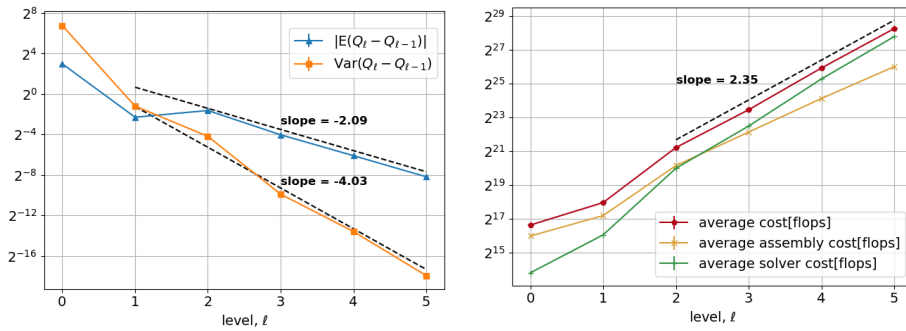


Figure 7: Example 1 with $\sigma^2 = 1$ using AMLMC. Left: Mean and variance of $Q_\ell - Q_{\ell-1}$ for level ℓ , with a 95% confidence interval. Right: The average work per sample (measured in flops) for level ℓ .

growth of W_ℓ for SMLMC and AMLMC in Example 1 with $\sigma^2 = 4$. We observed the mean and variance of AMLMC converges twice faster than SMLMC again. Moreover, with the same number of samples, AMLMC displays a more stable variance convergence than SMLMC.

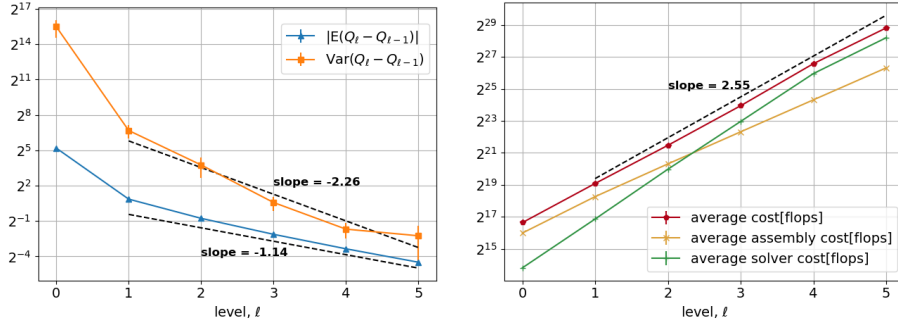


Figure 8: Example 1 with $\sigma^2 = 4$ using SMLMC. Left: Mean and variance of $Q_\ell - Q_{\ell-1}$ for level ℓ , with a 95% confidence interval. Right: The average work per sample (measured in flops) for level ℓ . The cost of SMLMC on this example does not depend on σ , but for easy reference we duplicate the graphs from Figure 6 here.

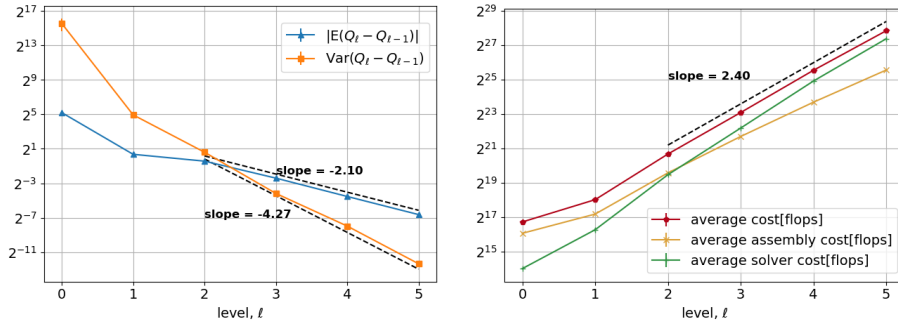


Figure 9: Example 1 with $\sigma^2 = 4$ using AMLMC. Left: Mean and variance of $Q_\ell - Q_{\ell-1}$ for level ℓ , with a 95% confidence interval. Right: The average work per sample (measured in flops) for level ℓ .

Figure 10 shows the estimated MLMC work complexity against the given tolerance TOL. Figure 10a and 10b show the average MLMC work W (measured in flops) against TOL for $\sigma^2 = 1$ and $\sigma^2 = 4$. With increase in variance, there is a fine distinction between the work complexity of the both schemes. To reveal or exclude the logarithmic term in the MLMC complexity, the quantity $\sqrt{W \cdot \text{TOL}^2}$ against TOL is shown in Figure 10c and 10d. When $W \propto \text{TOL}^{-2} \log^2(\text{TOL})$, $\sqrt{W \cdot \text{TOL}^2} \propto \log(\text{TOL})$. In both Figure 10c and 10d, the line plot of SMLMC grows linearly. The results show that the slope for the case $\sigma^2 = 4$ is larger than for $\sigma^2 = 1$, whereas the line plot of AMLMC does not demonstrate a dependence on TOL as TOL decreases.

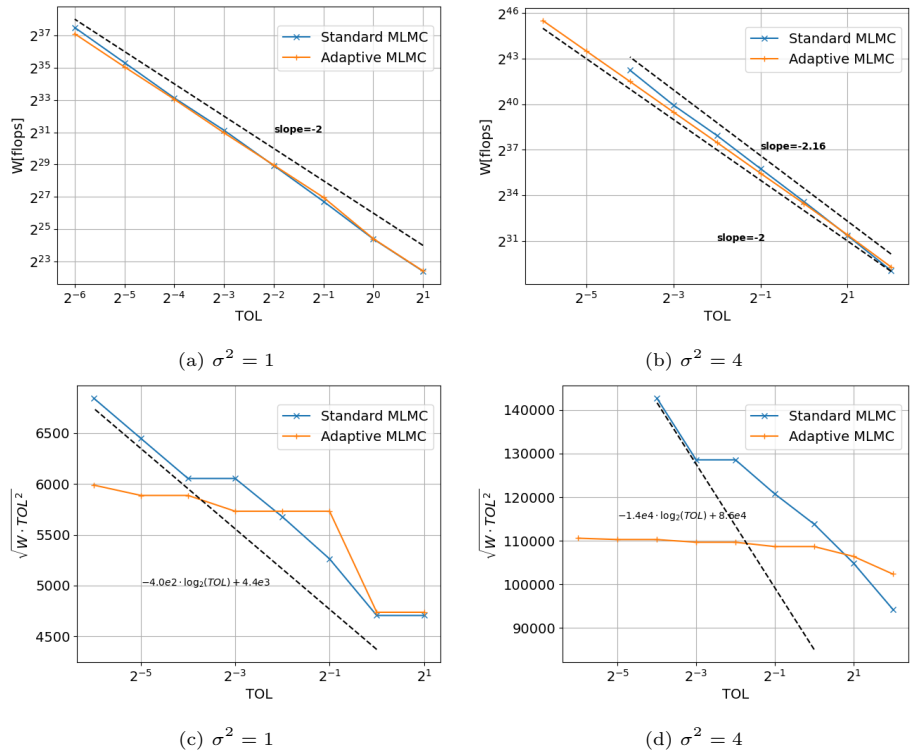


Figure 10: Example 1: Estimated MLMC work W (in flops) (10a, 10b) and $\sqrt{W \cdot \text{TOL}^2}$ (10c, 10d) versus error tolerance TOL for SMLMC and AMLMC for two variances in Example 1.

In Figure 11, we verified the accuracy of our MLMC algorithm by comparing the errors of the MLMC estimator and the given TOL. The errors were computed against a reference value, which is approximately 38.7, given by an AMLMC estimator with $\text{TOL} = 2^{-6}$. For all cases except the largest considered TOL for SMLMC, the percentage of samples having larger errors than their prescribed TOL was $< 5\%$. The result is consistent with our choice of 95% success probability.

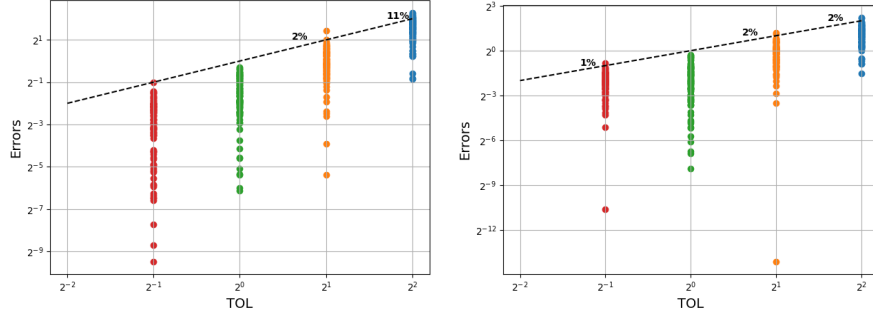


Figure 11: Example 1 with $\sigma^2 = 4$: Estimated error for four TOL values with SMLMC (Left) and AMLMC (Right). The reference line is for when TOL equals to the estimated error, and the percentages are calculated from the number of estimator realizations for which the estimated error is above TOL.

4.3.3. Example 2

Now let a be a lognormal random field

$$a(x, \omega) = \exp\left(\sum_{i=0}^{I-1} \xi_i(\omega) \sqrt{\lambda_i} \theta_i(x)\right), \quad x \in D, \quad (41)$$

with $I = 256$ terms, where ξ_i are i.i.d. $\mathcal{N}(0, 1)$ and λ_i are Fourier coefficients corresponding to trigonometric basis functions θ_i in the Fourier expansion of the Matérn covariance

$$C(h) = \frac{\sigma^2}{2^{\nu-1} \Gamma(\nu)} \left(\sqrt{2\nu} \frac{h}{r}\right)^\nu K_\nu\left(\sqrt{2\nu} \frac{h}{r}\right), \quad h \geq 0, \quad (42)$$

with correlation length $r = 1$ and smoothness parameter $\nu = 6.5$, where Γ is the gamma function and K_ν is the modified Bessel function of the second kind. The Fourier coefficients, arranged in descending order, have the decay $\lambda_i \leq C i^{1+\frac{2\nu}{d}}$; see [9]. The connection to the Matérn covariance with these choices of ν and r holds because the latter yields the random field pathwise $C^3(\mathcal{D})$ regularity; see [86]. This in turn ensures that $u(\cdot, \omega)$ and $\varphi(\cdot, \omega) \in C^3(\mathcal{D})$, as required for computing the error density [64, 65]. Figure 12 shows a few random field realizations for $\sigma^2 = 1$ and $\sigma^2 = 4$.

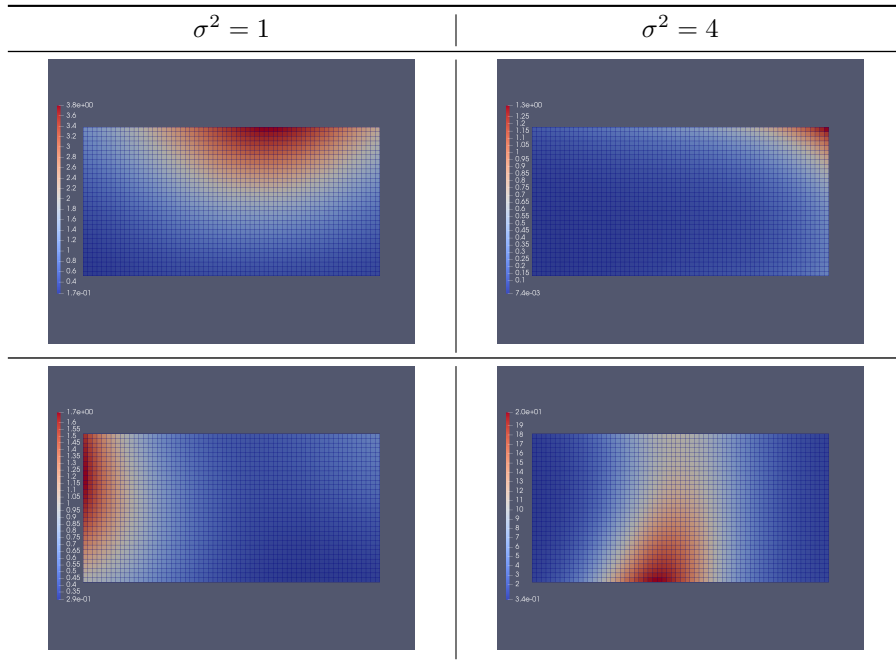


Figure 12: Example 2 with $\sigma^2 = 1$ (Left) and $\sigma^2 = 4$ (Right): A few realizations of the random field a (41)

Here, the pathwise regularity of the coefficient $a(\cdot, \omega)$ is sufficient to make the numerical quadrature error negligible in our computations, even on the coarsest mesh.

Many studies on sampling Gaussian random fields have been reported, see [28, 31, 37, 41, 57–59, 87]. The θ_i , λ_1 , and ξ_i used are obtained from the Fourier series expansion method as proposed in [9] and considered as a continuous version of the circulant embedding approach [26, 37]. The method first periodically extends the covariance operator C and then the Fourier coefficients $\{\lambda_i\}$ of the covariance operator can be efficiently computed.

In Example 2, we chose $\text{TOL}_\ell = 2 \cdot 4^{-\ell}$ and $\text{TOL}_\ell = 4^{1-\ell}$ for the AMLMC cases $\sigma^2 = 1$ and $\sigma^2 = 4$, respectively.

Figures 13 and 14 show the $L^1(\mathcal{D})$ norms and $L^{\frac{1}{2}}(\mathcal{D})$ quasi-norms of the samples from Example 2 with $\sigma^2 = 1$ and $\sigma^2 = 4$, respectively. As shown in Figure 4, the $L^{\frac{1}{2}}(\mathcal{D})$ quasi-norms remain stable across meshes, while the $L^1(\mathcal{D})$ norms grow with the rate h_s^{-1} .

Figures 15 and 16 show the convergence of mean E_ℓ and variance V_ℓ , and the cost growth W_ℓ in Example 2 with $\sigma^2 = 1$ for SMLMC and AMLMC. Figure 17, and 18 give the result with $\sigma^2 = 4$. In Example 2, the cost is dominated by the assembly caused by the random fields that were generated.

Figures 13-18 are comparable to the corresponding figures in Example 1, demonstrating that SMLMC and AMLMC have similar behaviors as in Exam-

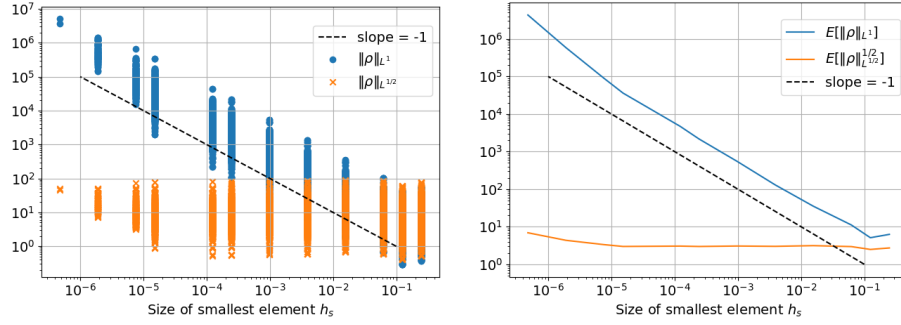


Figure 13: Example 2 with $\sigma^2 = 1$: $L^1(\mathcal{D})$ norm and $L^{\frac{1}{2}}(\mathcal{D})$ quasi-norms of the error density ρ (left) and the expected value of the norms and quasi-norms on each mesh (right) against the size of the smallest element h_s on a hierarchy of adaptive meshes (Figure 2).

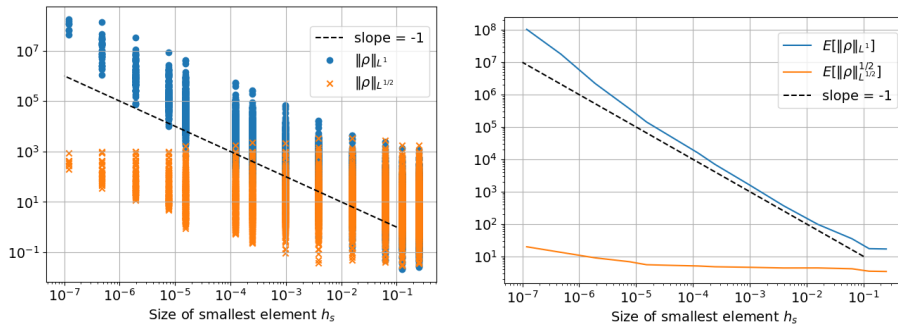


Figure 14: Example 2 with $\sigma^2 = 4$: $L^1(\mathcal{D})$ norm and $L^{\frac{1}{2}}(\mathcal{D})$ quasi-norms of the error density ρ (left) and the expected value of the norms and quasi-norms on each mesh (right) against the size of the smallest element h_s on a hierarchy of adaptive meshes (Figure 2).

ple 1.

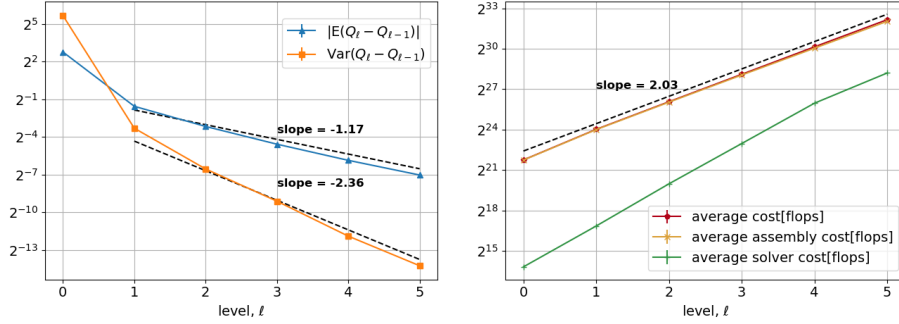


Figure 15: Example 2 with $\sigma^2 = 1$ using SMLMC. Left: Mean and variance of $Q_\ell - Q_{\ell-1}$ for level ℓ . Right: The average work per sample (measured in flops) for level ℓ .

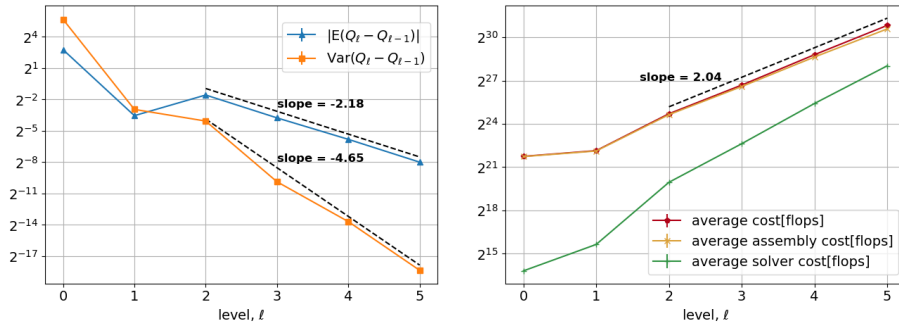


Figure 16: Example 2 with $\sigma^2 = 1$ AMLMC. Left: Mean and variance of $Q_\ell - Q_{\ell-1}$ for level ℓ . Right: The average work per sample (measured in flops) for level ℓ .

Similar to Figure 11, Figure 19 shows a graph of the errors computed against a reference value (~ 22.6), given by an AMLMC estimator with $\text{TOL} = 2^{-7}$. For all the cases except the largest considered TOL for AMLMC, the percentage of samples having larger errors than their prescribed TOL is $< 5\%$. This is consistent with our choice of 95% success probability.

Figure 20 shows the estimated MLMC work complexity against the given tolerance TOL . Figures 20a and 20b show the work W (measured in flops) against TOL for $\sigma^2 = 1$ and $\sigma^2 = 4$. The increase in variance shows a fine distinction between the work complexity of both schemes. To reveal or rule out the logarithmic term in the MLMC complexity, the quantity $\sqrt{W} \cdot \text{TOL}^2$ against TOL is shown in Figures 20c and 20d. When $W \propto \text{TOL}^{-2} \log^2(\text{TOL})$ and $\sqrt{W} \cdot \text{TOL}^2 \propto \log(\text{TOL})$. In both figures, the line plot of SMLMC grows linearly. The results show that the slope for the case $\sigma^2 = 4$ is larger than $\sigma^2 = 1$, whereas the line plot of AMLMC does not demonstrate a dependence on TOL .

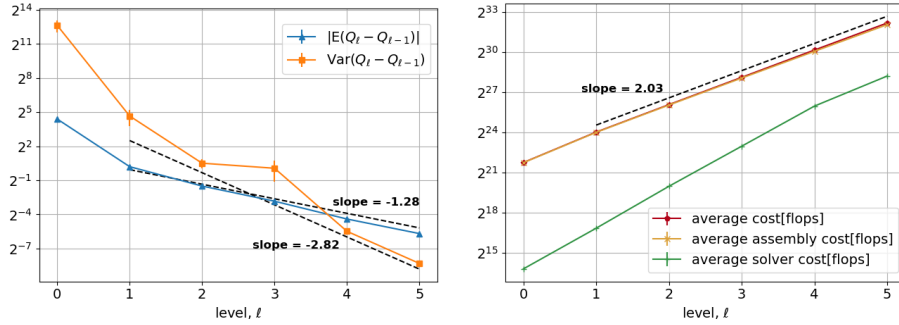


Figure 17: Example 2 with $\sigma^2 = 4$ using SMLMC. Left: Mean and variance of $Q_\ell - Q_{\ell-1}$ for level ℓ . Right: The average work per sample (measured in flops) for level ℓ .

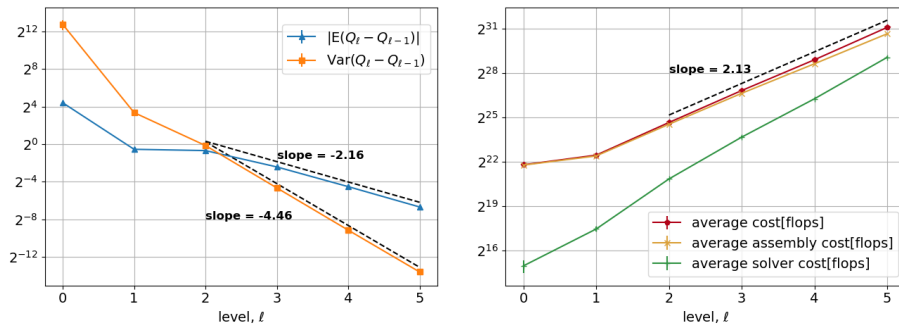


Figure 18: Example 2 with $\sigma^2 = 4$ using AMLMC. Left: Mean and variance of $Q_\ell - Q_{\ell-1}$ for level ℓ . Right: The average work per sample (measured in flops) for level ℓ .

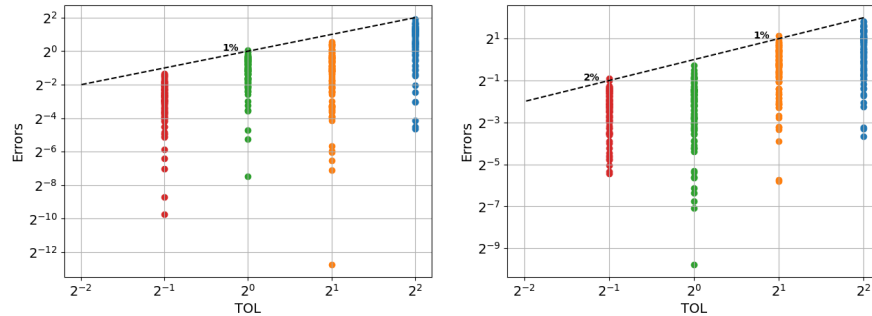
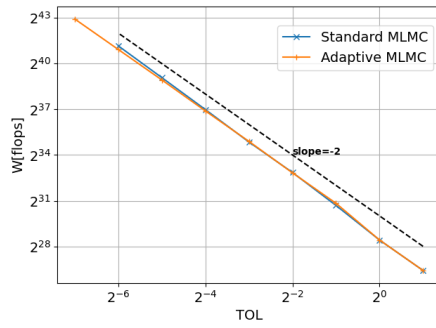
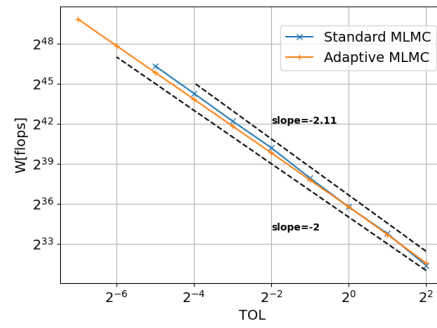


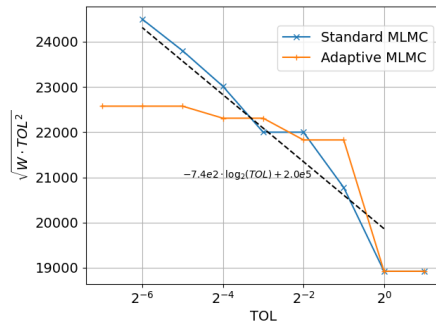
Figure 19: Example 2 with $\sigma^2 = 4$. Estimated error for four TOL values with SMLMC (left) and AMLMC (right). The reference line shows when TOL equals the estimated error, and the percentages are calculated using the number of estimator realizations for which the estimated error is above TOL.



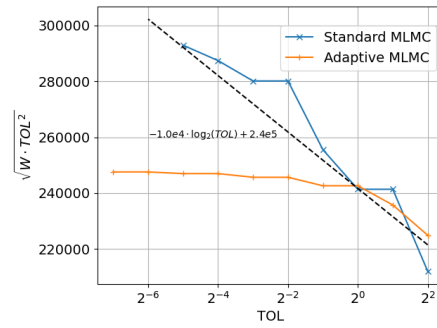
(a) $\sigma^2 = 1$



(b) $\sigma^2 = 4$



(c) $\sigma^2 = 1$



(d) $\sigma^2 = 4$

Figure 20: Example 2. Estimated MLMC work W (in flops) (20a, 20b) and $\sqrt{W \cdot \text{TOL}^2}$ (20c, 20d) against error tolerance TOL for SMLMC, and AMLMC for two variances $\sigma^2 = 1$ and $\sigma^2 = 4$.

Figure 21 plots the histograms of coarse-fine mesh level of AMLMC in Example 2 with $\sigma^2 = 1$ for level $\ell = 1, 2, 3, 4, 5$. Because the coarse-fine pair in our MLMC scheme uses the same random field, $\Delta Q_\ell(\omega) = (Q_\ell - Q_{\ell-1})(\omega)$ if the coarse mesh level equals the fine mesh level, thus reducing the efficiency of MLMC. With increasing ℓ , the fraction of zero samples ($\Delta Q_\ell(\omega) = 0$) reduces and disappears starting from $\ell = 2$.

Figure 22 plots the histograms of coarse-fine mesh level of AMLMC in Example 2 with $\sigma^2 = 4$ for level $\ell = 1, 2, 3, 4, 5$. Similar to the previous example, the fraction of zero samples ($\Delta Q_\ell(\omega) = 0$) reduces with an increasing ℓ , and disappears starting from $\ell = 3$. The samples satisfying a particular error estimate are extensively distributed into many auxiliary meshes, indicating that computing samples on a fixed mesh, as in SMLMC or using a batch adaptive approach, is less efficient.

Level, ℓ	0	1	2	3	4	5
SMLMC	2.48e+4	2.50e+3	1.66e+3	1.07e+3	9.04e+2	8.40e+2
AMLMC	2.51e+4	1.67e+3	2.19e+3	5.67e+2	2.95e+2	1.19e+2

Table 2: Example 2 with $\sigma^2 = 1$: The values $\sqrt{V_\ell W_\ell}$ for the considered MLMC estimators.

Level, ℓ	0	1	2	3	4	5
SMLMC	3.15e+5	3.65e+4	1.54e+4	9.84e+3	8.08e+3	1.06e+4
AMLMC	3.38e+5	1.41e+4	6.09e+3	2.75e+3	1.13e+3	5.17e+2

Table 3: Example 2 with $\sigma^2 = 4$: The values $\sqrt{V_\ell W_\ell}$ for the considered MLMC estimators.

ℓ	1	2	3	4	5
$\sigma^2 = 1$	0.31	2.42	0.77	0.91	0.56
$\sigma^2 = 4$	0.98	1.54	0.89	0.75	0.56

Table 4: Example 2 for AMLMC: The expected ratio of the computed variance $\text{Var}(Q_\ell - Q_{\ell-1})$ to the corresponding estimated variance derived from (32). The ratios are of $\mathcal{O}(1)$, indicating a sharp enough error estimate.

In Table 2 and 3, the values $\sqrt{V_\ell W_\ell}$ are the largest in level $\ell = 0$. The estimated MLMC work $W = \text{TOL}^{-2} (\sum_{\ell=0}^L \sqrt{V_\ell W_\ell})^2$. In both cases, the quantity $\sqrt{V_\ell C_\ell}$ in AMLMC decays like a geometric sequence, while such quantity is asymptotically equally distributed in SMLMC, indicating the logarithmic dependence of TOL in the SMLMC complexity. The logarithmic term in the complexity is revealed in Figures 20c and 20d. This confirms the theoretical complexity prediction of TOL^{-2} for AMLMC and $\text{TOL}^{-2} \log^2(\text{TOL}^{-1})$ for SMLMC.

To confirm that our asymptotic complexity predictions are accurate, cf. Corollary 1, the computational variances across levels must be close to their corresponding ones based on (32). Table 4 shows that for Example 2 in Section 4.3.3 the estimated variances are sufficiently sharp, even for coarse levels.

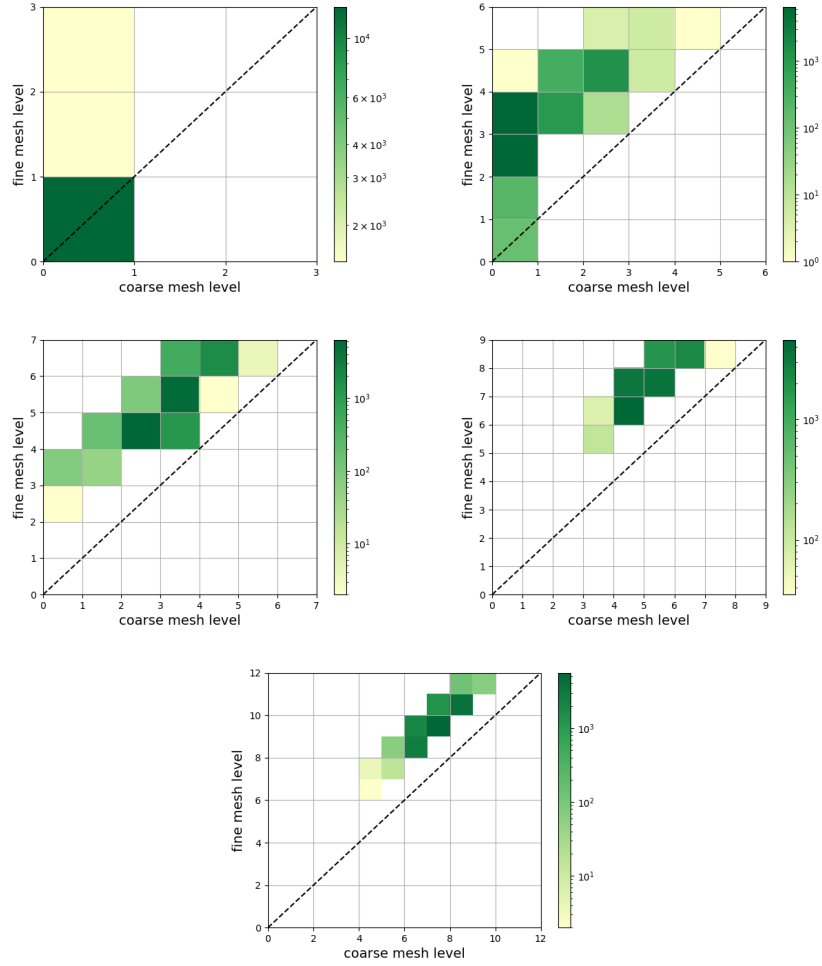


Figure 21: Example 2 with $\sigma^2 = 1$ using AMLMC: Stochastic stopping of coarse-fine pairs for the mesh level ℓ . Top: $\ell = 1, 2$ from left to right. Middle: $\ell = 3, 4$ from left to right. Bottom: $\ell = 5$. In each subplot, the dashed diagonal line denotes where the coarse mesh level equals the fine mesh level.

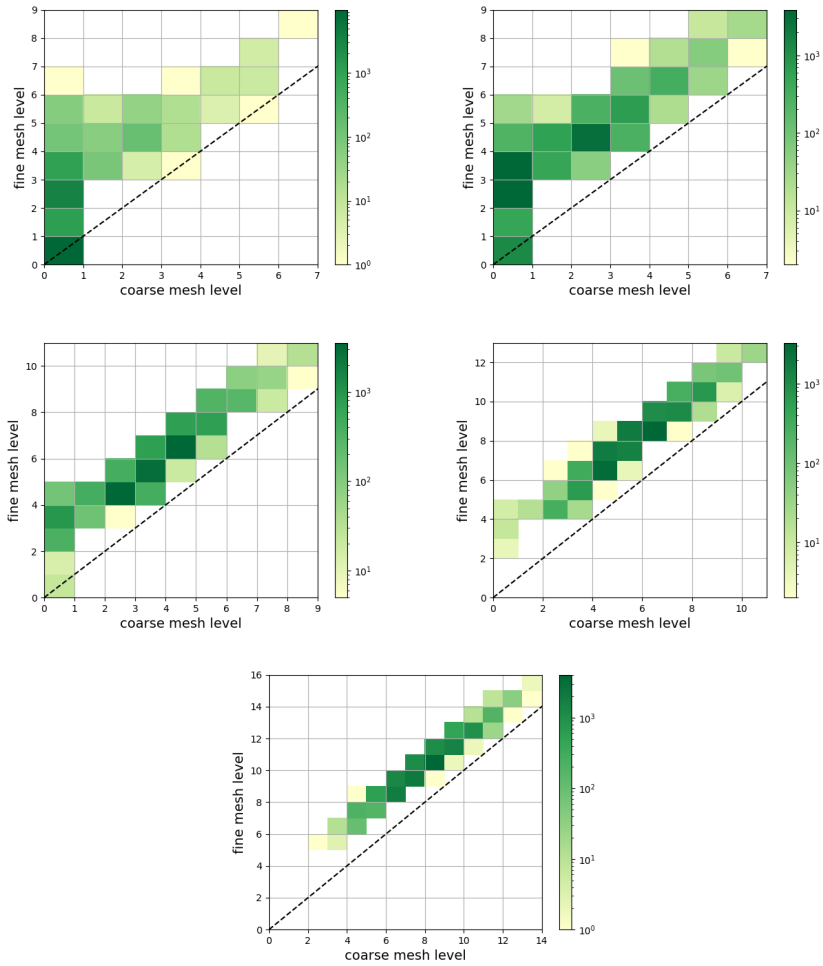


Figure 22: Example 2 with $\sigma^2 = 4$ using AMLMC: Stochastic stopping of coarse-fine pairs for the mesh level ℓ . Top: $\ell = 1, 2$ from left to right. Middle: $\ell = 3, 4$ from left to right. Bottom: $\ell = 5$.

5. Conclusions

We proposed an AMLMC for goal-oriented approximation in a linear elliptic PDE with geometric singularities and a lognormal random diffusivity coefficient. We built our AMLMC on [65], which developed weak convergence rates for an adaptive algorithm using isoparametric d-linear quadrilateral finite element approximations and the dual weighted residual error representation in a deterministic setting. This theory provided us with sharp error estimates and indicators that guide the creation of a locally refined mesh sequences, tuned to the singularity at hand. First, as a preparation phase, a sequence of deterministic h -adaptive auxiliary meshes was precomputed to satisfy a sequence of tolerances, using a deterministic approximation of the coefficient a , for instance, $\exp(\mathbb{E}[\log(a)])$. This step has a negligible cost and creates deterministic refinements that capture the geometry-driven singularities in the problem.

Then, each sample on a level in the MLMC hierarchy selects the coarsest auxiliary mesh such that a sample-dependent, *a posteriori* error estimate-based stopping criterion is satisfied. The error contributions are in general not equally distributed among samples to achieve optimal approximation. Rather, they are subject to a scaling factor that may be unbounded in the lognormal case. Compared with a batch-adaptive MLMC, for instance in [27, 71], our method circumvents the cost of generating meshes using a batch of realizations, based on the assumption that the error density blows up in a fixed location, as in our case of geometrically driven singularities. Furthermore, using stochastic meshes, our approach is more efficient than a batch adaptive algorithm when there is a lack of uniform coercivity, such as in the lognormal case. Moreover, our approach specifically avoids the costly overhead of building adaptive meshes from scratch for each realization. Instead, we only need to check a stopping criterion within the sequence of auxiliary meshes, which are already available.

Furthermore, when the solving cost is higher than the assembly cost, we discuss the use of iterative solvers and compare their efficiency with direct ones. To save computational work, we proposed a goal-oriented stopping criterion for the iterative solver, the realization of the diffusivity coefficient, and the desired level of AMLMC approximation.

Theoretically, the error density characterizes the cases where adaptivity provides a noticeable advantage, namely, those where the error density blows up in $L^1_P(\mathcal{D} \times \Omega)$, as we refine the mesh around the singularities, cf Theorem 1 and Corollary 1.

We worked with a finite Fourier expansion for the log diffusivity coefficient in our 2D numerical experiments. Note that this expansion is not the only way to represent a field. Our adaptive method can also work with other representations, see, for instance, the work [23]. In our numerical experiments, we observed efficiency improvements compared with both standard MC and MLMC for a singularity similar to that at the tip of a slit modeling a crack. We compared AMLMC with SMLMC for log fields with variances $\sigma^2 = 1$ and $\sigma^2 = 4$, respectively. In these examples, the error density-based error estimates are sharp. They accurately predict both the bias error and the variances across lev-

els, indicating that the asymptotic theory is relevant to analyzing the observed behavior of our AMLMC. Although the observed complexity of the SMLMC deteriorates with the increase in variance, our AMLMC complexity remains stable between these two variances. Consistent with the theoretical results, the observed complexity for those 2D cases is TOL^{-2} for AMLMC, $\text{TOL}^{-2} \log^2(\text{TOL})$ for SMLMC, TOL^{-3} for AMC, and TOL^{-4} for MC. We predict further gains favoring AMLMC for larger values of dimension d . We note in passing that the uniform refinements fail to produce a sharp error estimate, even when coupled with the same error estimate that is sharp when using adaptive refinements. This makes the adaptive approach more attractive because it produces more robust and accurate results. Furthermore, when achieving the TOL^{-2} complexity, our AMLMC can be directly coupled with the popular unbiased MLMC approach introduced in [60, 84], simply by randomizing over the sequence of tolerances used to create the adaptive levels.

The pointwise convergence of the error density proved in [65] is the crucial theoretical component of our approach. The theoretical analysis of the error density convergence relies on proper local averaging and the multilinear structure of the isoparametric d-linear quadrilateral finite elements with hanging nodes. Hanging nodes are important to provide sufficient flexibility in the mesh refinements. The efficient computation of local averages in the error estimate is a contribution to this work, improving on [65]. The pointwise convergence of the error density is fundamental to demonstrating the theoretical results on stopping, asymptotic accuracy, and efficiency, as proved in [65], and is inherited by our AMLMC. However, the theoretical convergence of the error density also requires the solution and its dual to have $C^3(\mathcal{D})$ pathwise regularity. As reported in [65], this is not a practical limitation. A sequence of regularized geometries (for example by rounding a reentrant corner with a small radius) can be produced that satisfies the $C^3(\mathcal{D})$ assumptions and converges to our problem, showing up the $L^1(\mathcal{D})$ explosion of the error density, which governs the complexity of SMLMC, and the uniform boundedness of the quasi-norm, corresponding to the AMLMC. In practice, regularization is not required to produce accurate error estimates and a stable estimate of error density.

Acknowledgements

This publication is based on work supported by the Alexander von Humboldt Foundation and the King Abdullah University of Science and Technology (KAUST) office of sponsored research (OSR) under Award No. OSR-2019-CRG8-4033. The authors thank Daniele Boffi and Alexander Litvinenko for fruitful discussions. We also acknowledge the use of the following open-source software packages: `deal.II` [4], `PAPI` [90].

Appendix A. Algorithm Listings

We list the algorithms and corresponding notations below.

Algorithm 1: Primal and dual solvers iteration

Input: Iteration solver tolerance TOL_{iter} , primal iteration operator \mathcal{A}_p , dual iteration operator \mathcal{A}_d , initial vector $u^{(0)}$ and $\varphi^{(0)}$, primal linear system A_p and right-hand side b_p , dual linear system A_d and right-hand side b_d .

Output: Primal solution u_{iter} and dual solution φ_{iter}

Set PrimalSolver = *true*

Set DualSolver = *true*

Set iteration step $k = 0$

while PrimalSolver || DualSolver **do**

 Proceed the primal iteration $u^{(k+1)} = \mathcal{A}_p u^{(k)}$

 Proceed the dual iteration $\varphi^{(k+1)} = \mathcal{A}_d \varphi^{(k)}$

 Compute primal residual $r_p^{(k+1)} = b_p - A_p u^{(k+1)}$

 Compute dual residual $r_d^{(k+1)} = b_d - A_d \varphi^{(k+1)}$

if $|(r_p^{(k+1)}, \varphi^{(k+1)})| < \text{TOL}_{\text{iter}}$ **then**

 | Set PrimalSolver = *false*

end

if $|(r_d^{(k+1)}, u^{(k+1)})| < \text{TOL}_{\text{iter}}$ **then**

 | Set DualSolver = *false*

end

 Set $k = k + 1$

end

Algorithm 2: Adaptive generation of an auxilliary mesh hierarchy

Input: $\{\text{TOL}_\ell\}_{\ell=0}^L, \mathcal{H}_{-1}, L, \overline{N}_{-1}, C_R, C_S, c, a$

Output: Mesh hierarchy $\{\mathcal{H}_\ell\}_{\ell=0}^L$

Initialize the mesh \mathcal{H}_{-1} and the parameter $\overline{N}_{-1} = N_{-1}$, with N_{-1} the number of cells on mesh \mathcal{H}_{-1}

```
for  $\ell = 0, 1, \dots, L$  do
  keepRefining = TRUE
   $\mathcal{H}_\ell = \mathcal{H}_{\ell-1}$ 
   $\overline{N}_\ell = c\overline{N}_{\ell-1}$ 
  while keepRefining do
    Assemble the primal and dual linear system using the coefficient
     $a$  on mesh  $\mathcal{H}_\ell$ 
    Solve the primal and dual problem (1) using Algorithm 1, with
     $\text{TOL}_{\text{iter}} = \frac{1}{10}\text{TOL}_\ell$ 
    Compute approximate error density  $\bar{\rho}$  (37), error indicator  $r$ 
    (A.1) and the error estimate  $e_{\text{est}}$  (A.2)
    if Stopping condition (A.4) is not satisfied then
      foreach cell  $k \in \mathcal{T}$  do
        if  $r(k)$  meets the refinement criterion (A.5) then
          | Mark the cell  $k$  for refinement
        end
      end
      Mark the cells for refinement to satisfy the mesh constraints
      Refine the marked cells on mesh  $\mathcal{H}_\ell$ 
      Update the number of cells  $N_\ell$  on mesh  $\mathcal{H}_\ell$  and set
       $\overline{N}_\ell = \max\{\overline{N}_\ell, N_\ell\}$ 
    else
      | Set keepRefining = FALSE
    end
  end
end
end
```

The error indicator for cell K , using the approximated error density $\bar{\rho}$ (37), is given by,

$$r(K) = \bar{\rho}_K h_K^{2+d}. \quad (\text{A.1})$$

The error estimate e_{est} is the summation of all local error indicators,

$$e_{\text{est}} = \sum_K r(K). \quad (\text{A.2})$$

The absolute error estimate $e_{\text{est, abs}}$ sums up all unsigned local error indicators,

$$e_{\text{est, abs}} = \sum_K |r(K)|. \quad (\text{A.3})$$

The stopping condition in Algorithm 2 is to control the largest error indicator,

$$\max_{1 \leq K \leq N_\ell} r(K) < C_S \frac{\text{TOL}_\ell}{\mathcal{N}_\ell}. \quad (\text{A.4})$$

The stopping condition controls the maximal error indicator for a fast decay [64, 65]). Note that N_ℓ is the number of cells on mesh level ℓ , whereas the variable \mathcal{N}_ℓ is introduced to control the refinement and stopping.

The refinement criterion in Algorithm 2 for cell K , $K = 1, 2, \dots, N_\ell$, is to refine the cells with error indicators greater or equal to a threshold,

$$r(K) \geq C_R \frac{\text{TOL}_\ell}{\mathcal{N}_\ell}. \quad (\text{A.5})$$

In Algorithm 3, the computed stochastic scaling factor $K_k(\omega)$ on mesh k is given by,

$$K_k(\omega) = \frac{\int_{\mathcal{D}} \bar{\rho}_k(x; \omega)^{\frac{d}{p+d}} dx}{\int_{\mathcal{D}} \mathbb{E} \left[\bar{\rho}_0^{\frac{d}{p+d}} \right]}, \quad (\text{A.6})$$

where in Section 4 the denominator was estimated on the coarsest mesh 0. Generally, we propose to use an MLMC estimate of $\int_{\mathcal{D}} \mathbb{E} \left[\bar{\rho}_0^{\frac{d}{p+d}} \right]$ using an iterative update procedure. We listed Algorithm 3 as selecting specific solvers but in general, the user can choose the solvers in another way to optimize efficiency.

Appendix B. Mesh function optimizations

This appendix contains the calculations resulting in the optimal stochastic mesh size functions in (19)

Algorithm 3: One sample of $\Delta Q_\ell = Q_\ell - Q_{\ell-1}$ in AMLMC

Input: ℓ , $\text{TOL}_{\text{bias},\ell}$, $\{(\mathcal{H}_k, a_k)\}_{k=0}^\infty$
Output: One sample of $(Q_\ell, Q_{\ell-1})$
Set $k = 0$
Set error estimate $e_{\text{est}} = +\infty$
Set $\text{CoarseFlag} = \text{true}$
while true **do**
 Generate the random field a_k on mesh \mathcal{H}_k
 if $k == 0$ **then**
 | Compute u_k and φ_k from (1) and a direct solver UMFPACK [24]
 else
 | Set the iterative solver tolerance
 | $\text{TOL}_{\text{iter}} = \frac{1}{10} K_{k-1}(\omega) \cdot \text{TOL}_{\text{bias},\ell}$
 | Compute u_k and φ_k from (1) and Algorithm 1, with the iterative
 | solver tolerance TOL_{iter}
 end
 Compute e_{est} using (37), (A.1) and (A.2)
 Compute $K_k(\omega)$ using (A.6)
 if $\ell = 0$ **then**
 | Set $Q_{\ell-1} = 0$
 | Set $\text{CoarseFlag} = \text{false}$
 end
 if $e_{\text{est}} < K_k(\omega) \cdot \text{TOL}_{\text{bias},\ell-1} \wedge \text{CoarseFlag}$ **then**
 | Set $Q_{\ell-1} = Q(u_k)$
 | Set $\text{CoarseFlag} = \text{false}$
 end
 if $e_{\text{est}} < K_k(\omega) \cdot \text{TOL}_{\text{bias},\ell}$ **then**
 | Set $Q_\ell = Q(u_k)$
 | break;
 end
 Set $k = k + 1$
end

Algorithm 4: Assemble y -line structures from a quadtree

Input: Quadtree of cells \mathcal{T}

Output: Dictionary \mathcal{D} of vertices lines \mathcal{L} , where the vertices of each line have the same y coordinate

Function ASSEMBLE-LINE(\mathcal{V}):

 Create empty vector of cells $\mathcal{V}_{\text{Left}}$ and $\mathcal{V}_{\text{Right}}$

foreach $Cell \in \mathcal{V}$ **do**

if $Cell$ has children **then**

$\mathcal{V}_{\text{Left}}$ push back $Cell \rightarrow \text{child}(0)$

$\mathcal{V}_{\text{Left}}$ push back $Cell \rightarrow \text{child}(1)$

$\mathcal{V}_{\text{Right}}$ push back $Cell \rightarrow \text{child}(2)$

$\mathcal{V}_{\text{Right}}$ push back $Cell \rightarrow \text{child}(3)$

else

$\mathcal{V}_{\text{Left}}$ push back $Cell$

end

end

 Create empty lines of vertices $\mathcal{L}_{\text{Bottom}}$ and \mathcal{L}_{Top}

if All cells $\in \mathcal{V}$ have no children **then**

if All cells $\in \mathcal{V}$ have the same size **then**

foreach $Cell \in \mathcal{V}$ **do**

$\mathcal{L}_{\text{Bottom}}$ push back $Cell \rightarrow \text{vertex}(0)$

\mathcal{L}_{Top} push back $Cell \rightarrow \text{vertex}(2)$

end

else

foreach $Cell \in \mathcal{V}$ **do**

$\mathcal{L}_{\text{Bottom}}$ push back $Cell \rightarrow \text{vertex}(0)$

end

end

if $\mathcal{L}_{\text{Bottom}}$ or \mathcal{L}_{Top} has y coordinate already in dict. \mathcal{D} **then**

 Merge with the existing line in \mathcal{D}

else

 Save $\mathcal{L}_{\text{Bottom}}$ and \mathcal{L}_{Top} in the dictionary \mathcal{D}

end

return

else

 ASSEMBLE-LINE($\mathcal{V}_{\text{Left}}$)

if $\mathcal{V}_{\text{Right}}$ is non-empty **then**

 ASSEMBLE-LINE($\mathcal{V}_{\text{Right}}$)

end

end

end

Create vector \mathcal{V} , containing the tree root cell $\mathcal{T} \rightarrow \text{root}$

ASSEMBLE-LINE(\mathcal{V})

Optimal stochastic, adaptive, mesh functions. We examine the ideal stochastic mesh size function, $h(x; \omega)$, which minimizes the work model (17) subject to the constraint that the bias model (18) equals TOL_{bias} . For this purpose, we introduce the Lagrangian,

$$\mathcal{L}(h; \lambda) = \int_{\mathcal{D}} \mathbb{E}[h^{-d}] + \lambda \left(\int_{\mathcal{D}} \mathbb{E}[\rho h^p] - \text{TOL}_{\text{bias}} \right). \quad (\text{B.1})$$

By considering the variation of the Lagrangian with respect to h , we obtain the optimality condition

$$-\frac{d}{h^{d+1}} + \lambda p \rho h^{p-1} \equiv 0 \quad \Leftrightarrow \quad h(x; \omega) = \left(\frac{1}{\lambda} \frac{d}{p} \rho(x; \omega)^{-1} \right)^{\frac{1}{p+d}}.$$

Then, using the bias constraint, we have

$$\text{TOL}_{\text{bias}} = \int_{\mathcal{D}} \mathbb{E} \left[\rho \left(\frac{1}{\lambda} \frac{d}{p} \rho^{-1} \right)^{\frac{p}{p+d}} \right],$$

we can determine the Lagrange multiplier,

$$\lambda^{-\frac{1}{p+d}} = \left(\frac{p}{d} \right)^{\frac{1}{p+d}} \frac{\text{TOL}_{\text{bias}}^{1/p}}{\left(\int_{\mathcal{D}} \mathbb{E} \left[\rho^{\frac{d}{p+d}} \right] \right)^{1/p}},$$

which after substituting back into the expression for $h(x; \omega)$ gives

$$h(x; \omega) = \frac{\text{TOL}_{\text{bias}}^{1/p}}{\left(\int_{\mathcal{D}} \mathbb{E} \left[\rho^{\frac{d}{p+d}} \right] \right)^{1/p}} \rho(x; \omega)^{-\frac{1}{p+d}},$$

as stated in (19).

Optimal stochastic, uniform, mesh functions. Restricting ourselves to constant mesh size functions, $h(x; \omega) \equiv h(\omega)$, corresponding to idealized uniform meshes, the Lagrangian in (B.1) becomes

$$\mathcal{L}(h; \lambda) = \mathbb{E} \left[h^{-d} \int_{\mathcal{D}} 1 \, dx \right] + \lambda \left(\mathbb{E} \left[h^p \int_{\mathcal{D}} \rho(x; \cdot) \, dx \right] - \text{TOL}_{\text{bias}} \right).$$

Introducing the constant $A = \int_{\mathcal{D}} 1 \, dx$, the area of D , and the random variable $R = \int_{\mathcal{D}} \rho(x; \cdot) \, dx$, the $L^1(D)$ -norm of $\rho(\cdot; \omega)$, and again taking variations with respect to h , the optimality condition is shown to be

$$-\frac{d}{h^{d+1}} A + \lambda R p h^{p-1} \equiv 0 \quad \Leftrightarrow \quad h(\omega) = \left(\frac{1}{\lambda} \frac{d}{p} \frac{A}{R(\omega)} \right)^{\frac{1}{p+d}}.$$

The bias constraint becomes

$$\text{TOL}_{\text{bias}} = \mathbb{E} \left[\left(\frac{1}{\lambda} \frac{d}{p} \frac{A}{R} \right)^{\frac{p}{p+d}} R \right],$$

from which we conclude

$$\lambda^{-\frac{1}{p+d}} = \left(\frac{p}{d} \frac{1}{A} \right)^{\frac{1}{p+d}} \frac{\text{TOL}_{\text{bias}}^{1/p}}{\mathbb{E} \left[R^{\frac{d}{p+d}} \right]^{1/p}}.$$

Substitution back in $h(\omega)$ yields,

$$h(\omega) = \text{TOL}_{\text{bias}}^{1/p} \frac{R(\omega)^{-\frac{1}{p+d}}}{\mathbb{E} \left[R^{\frac{d}{p+d}} \right]^{1/p}},$$

which using the definitions of A and R becomes (22).

Appendix C. Proof of Corollary 1

Associated with the work model (7) is the upper bound (11) where, since Assumption 2 is satisfied with $\kappa = C^{-1}$, $\gamma = d/p$, $q_s = 2$, and $q_w = 1$, the second term is asymptotically negligible as $\text{TOL} \rightarrow 0$. For the first term we obtain, assuming that V_0 is constant and $W_0 = \mathbb{E}[K_2] \text{TOL}_0^{-d/p}$ while using (32) and (33) for $\ell \geq 1$, in $\sum_{\ell=0}^L \sqrt{V_\ell W_\ell}$, that

$$\begin{aligned} & \left(\frac{C_\xi}{\theta \text{TOL}} \right)^2 \left(\sum_{\ell=0}^L \sqrt{W_\ell V_\ell} \right)^2 \\ &= \frac{K_3 K_5}{\text{TOL}^2} \text{TOL}_0^{-d/p} \underbrace{\left(\sqrt{\frac{V_0}{\text{Var}[K_1]}} \frac{1}{(C^{-1} - 1) \sqrt{1 + C^{d/p}}} + \text{TOL}_0 S \right)^2}_T, \quad (\text{C.1}) \end{aligned}$$

where

$$\begin{aligned} K_3 &= \mathbb{E}[K_2] \text{Var}[K_1], \\ K_5 &= \left(\frac{C_\xi}{\theta} \right)^2 (C^{-1} - 1)^2 (1 + C^{d/p}), \\ S &= \sum_{\ell=1}^L \left(C^{1 - \frac{d}{2p}} \right)^\ell = \begin{cases} L, & \text{if } d = 2p, \\ C^{1 - \frac{d}{2p}} \frac{1 - \left(C^{1 - \frac{d}{2p}} \right)^L}{1 - C^{1 - \frac{d}{2p}}}, & \text{if } d \neq 2p. \end{cases} \end{aligned}$$

To satisfy the bias constraint, $(1 - \theta) \text{TOL} \geq \text{TOL}_L = C^L \text{TOL}_0$, choose

$$L = \lceil L^* \rceil, \quad L^* = \log_C \left(\frac{1 - \theta}{\text{TOL}_0} \text{TOL} \right),$$

provided $\text{TOL}_0 > (1 - \theta) \text{TOL}$. Then $L^* \in \mathbb{R}^+$, since $C \in (0, 1)$.

Keeping TOL_0 fixed while letting $\text{TOL} \rightarrow 0$, one has three different situations depending on the asymptotic behavior of S :

If $d < 2p$, then $\left(C^{1-\frac{d}{2p}}\right)^L \rightarrow 0$ as $\text{TOL} \rightarrow 0$, so that T in (C.1) remains bounded and

$$\frac{W_{\text{MLMC}}}{\text{TOL}^{-2}} \rightarrow \frac{K_3 K_5}{\text{TOL}_0^{d/p}} \left(\sqrt{\frac{V_0}{\text{Var}[K_1]}} \frac{1}{(C^{-1} - 1) \sqrt{1 + C^{d/p}}} + \text{TOL}_0 \frac{C^{1-\frac{d}{2p}}}{1 - C^{1-\frac{d}{2p}}} \right)^2,$$

as $\text{TOL} \rightarrow 0$.

If $d = 2p$, then

$$\frac{L}{\log(\text{TOL}^{-1})} = \frac{1}{\log(\text{TOL}^{-1})} \left[\frac{\log(\text{TOL}^{-1}) + \log\left(\frac{\text{TOL}_0}{1-\theta}\right)}{\log(C^{-1})} \right] \rightarrow \frac{1}{\log(C^{-1})},$$

and

$$\frac{W_{\text{MLMC}}}{\text{TOL}^{-2} \log(\text{TOL}^{-1})^2} \rightarrow K_3 K_5 \text{TOL}_0^{-d/p} \log(C)^{-2},$$

as $\text{TOL} \rightarrow 0$.

If $d > 2p$, then

$$C^{(1-\frac{d}{2p})L^*} = \left(\frac{1-\theta}{\text{TOL}_0} \text{TOL} \right)^{(1-\frac{d}{2p})}.$$

Thus, allowing for the non-integer approximation L^* ,

$$\begin{aligned} \frac{S}{\text{TOL}^{1-\frac{d}{2p}}} &\rightarrow \left(\frac{1-\theta}{\text{TOL}_0} \right)^{(1-\frac{d}{2p})} \frac{1}{1 - C^{\frac{d}{2p}-1}}, \\ \frac{T}{\text{TOL}^{2-d/p}} &\rightarrow (1-\theta)^{2-d/p} \frac{1}{\left(1 - C^{\frac{d}{2p}-1}\right)^2}, \end{aligned}$$

and

$$\frac{W_{\text{MLMC}}}{\text{TOL}^{-d/p}} \rightarrow K_3 K_5 \frac{(1-\theta)^{2-d/p}}{\left(1 - C^{\frac{d}{2p}-1}\right)^2},$$

as $\text{TOL} \rightarrow 0$.

Together, the previous three cases show the limits of Corollary 1, allowing for non-integer L when $d > 2p$. Taking the integer constraint into account, it

follows from $L^* \leq L < L^* + 1$ that

$$\liminf_{\text{TOL} \rightarrow 0} \frac{W_{\text{MLMC}}}{\text{TOL}^{-d/p}} \geq K_3 K_5 \frac{(1-\theta)^{2-d/p}}{\left(1 - C^{\frac{d}{2p}} - 1\right)^2},$$

$$\limsup_{\text{TOL} \rightarrow 0} \frac{W_{\text{MLMC}}}{\text{TOL}^{-d/p}} \leq K_3 K_5 \frac{(1-\theta)^{2-d/p}}{\left(1 - C^{\frac{d}{2p}} - 1\right)^2} C^{1-\frac{d}{2p}}.$$

References

- [1] M. AINSWORTH AND J. T. ODEN, *A procedure for a posteriori error estimation for h-p finite element methods*, Computer Methods in Applied Mechanics and Engineering, 101 (1992), pp. 73–96.
- [2] ———, *A Posteriori Error Estimators for the Stokes and Oseen Equations*, SIAM Journal on Numerical Analysis, 34 (1997), pp. 228–245.
- [3] ———, *A Posteriori Error Estimation in Finite Element Analysis*, John Wiley Sons, Inc., 2000.
- [4] D. ARNDT, W. BANGERTH, B. BLAIS, T. C. CLEVINGER, M. FEHLING, A. V. GRAYVER, T. HEISTER, L. HELTAI, M. KRONBICHLER, M. MAIER, P. MUNCH, J.-P. PELTERET, R. RASTAK, I. THOMAS, B. TURCK SIN, Z. WANG, AND D. WELLS, *The deal.II library, version 9.2*, Journal of Numerical Mathematics, 28 (2020), pp. 131–146.
- [5] I. BABUŠKA, F. NOBILE, AND R. TEMPONE, *A Stochastic Collocation Method for Elliptic Partial Differential Equations with Random Input Data*, SIAM Review, 52 (2010), pp. 317–355.
- [6] I. BABUŠKA, J. WHITEMAN, AND T. STROUBOULIS, *Finite elements: an introduction to the method and error estimation*, Oxford University Press, 2010.
- [7] ———, *Finite Elements: An Introduction to the Method and Error Estimation*, Oxford University Press, 2010.
- [8] M. BACHMAYR, A. COHEN, R. DEVORE, AND G. MIGLIORATI, *Sparse polynomial approximation of parametric elliptic PDEs. part ii: lognormal coefficients*, ESAIM: M2AN, 51 (2017), pp. 341–363.
- [9] M. BACHMAYR, A. COHEN, AND G. MIGLIORATI, *Representations of Gaussian random fields and approximation of elliptic PDEs with lognormal coefficients*, Journal of Fourier Analysis and Applications, 24 (2018), pp. 621–649.

- [10] W. BANGERTH AND R. RANNACHER, *Adaptive Finite Element Methods for Differential Equations*, Lectures in Mathematics, Birkhäuser, Basel, 2003.
- [11] A. BARTH, C. SCHWAB, AND N. ZOLLINGER, *Multi-level Monte Carlo finite element method for elliptic PDEs with stochastic coefficients*, Numerische Mathematik, 119 (2011), pp. 123–161.
- [12] E. B. BECKER, G. F. CAREY, AND J. T. ODEN, *Finite elements: an introduction*, vol. 1, Prentice Hall, 1981.
- [13] R. BECKER AND R. RANNACHER, *An optimal control approach to a posteriori error estimation in finite element methods*, Acta Numerica, 10 (2001), p. 1–102.
- [14] M. BEN ALAYA AND A. KEBAIER, *Central limit theorem for the multilevel Monte Carlo Euler method*, The Annals of Applied Probability, 25 (2015), pp. 211–234.
- [15] C. BEN HAMMOUDA, A. MORAES, AND R. TEMPONE, *Multilevel hybrid split-step implicit tau-leap*, Numerical Algorithms, (2016).
- [16] M. BÜRG AND M. NAZAROV, *Goal-oriented adaptive finite element methods for elliptic problems revisited*, Journal of Computational and Applied Mathematics, 287 (2015), pp. 125–147.
- [17] J. CHARRIER, *Strong and weak error estimates for elliptic partial differential equations with random coefficients*, SIAM Journal on Numerical Analysis, 50 (2012), pp. 216–246.
- [18] J. CHARRIER AND A. DEBUSSCHE, *Weak truncation error estimates for elliptic PDEs with lognormal coefficients*, Stochastic Partial Differential Equations: Analysis and Computations, 1 (2013), pp. 63–93.
- [19] J. CHARRIER, R. SCHEICHL, AND A. TECKENTRUP, *Finite element error analysis of elliptic PDEs with random coefficients and its application to multilevel Monte Carlo methods*, SIAM Journal on Numerical Analysis, 51 (2013), pp. 322–352.
- [20] W. CHEN, G. KESIDIS, T. MORRISON, J. T. ODEN, J. H. PANCHAL, C. PAREDIS, M. PENNOCK, S. ATAMTURKTUR, G. TEREJANU, AND M. YUKISH, *Uncertainty in Modeling and Simulation*, in Research Challenges in Modeling and Simulation for Engineering Complex Systems, R. Fujimoto, C. Bock, W. Chen, E. Page, and J. H. Panchal, eds., Springer International Publishing, 2017, pp. 75–86.
- [21] K. A. CLIFFE, M. B. GILES, R. SCHEICHL, AND A. L. TECKENTRUP, *Multilevel Monte Carlo methods and applications to elliptic PDEs with random coefficients*, Computing and Visualization in Science, 14 (2011), p. 3.

- [22] N. COLLIER, A.-L. HAJI-ALI, F. NOBILE, E. VON SCHWERIN, AND R. TEMPONE, *A Continuation Multilevel Monte Carlo Algorithm*, BIT Numerical Mathematics, 55 (2015), pp. 399–432.
- [23] M. CROCI, M. B. GILES, M. E. ROGNES, AND P. E. FARRELL, *Efficient white noise sampling and coupling for multilevel monte carlo with nonnested meshes*, SIAM/ASA Journal on Uncertainty Quantification, 6 (2018), pp. 1630–1655.
- [24] T. A. DAVIS, *Algorithm 832: UMFPACK V4.3 – an unsymmetric-pattern multifrontal method*, ACM Transactions on Mathematical Software (TOMS), 30 (2004), pp. 196–199.
- [25] L. DEMKOWICZ, J. T. ODEN, W. RACHOWICZ, AND O. HARDY, *Toward a universal h-p adaptive finite element strategy, part 1. Constrained approximation and data structure*, Computer Methods in Applied Mechanics and Engineering, 77 (1989), pp. 79–112.
- [26] C. R. DIETRICH AND G. N. NEWSAM, *Fast and exact simulation of stationary gaussian processes through circulant embedding of the covariance matrix*, SIAM Journal on Scientific Computing, 18 (1997), pp. 1088–1107.
- [27] M. EIGEL, C. MERDON, AND J. NEUMANN, *An Adaptive Multilevel Monte Carlo Method with Stochastic Bounds for Quantities of Interest with Uncertain Data*, SIAM/ASA Journal on Uncertainty Quantification, 4 (2016), pp. 1219–1245.
- [28] M. FEISCHL, F. KUO, AND I. SLOAN, *Fast random field generation with H-matrices*, Numerische Mathematik, 140 (2018), pp. 639–676.
- [29] D. FUENTES, D. LITTLEFIELD, J. T. ODEN, AND S. PRUDHOMME, *Extensions of goal-oriented error estimation methods to simulations of highly-nonlinear response of shock-loaded elastomer-reinforced structures*, Computer Methods in Applied Mechanics and Engineering, 195 (2006), pp. 4659–4680. John H. Argyris Memorial Issue. Part I.
- [30] R. H. GALLAGHER, J. T. ODEN, AND O. C. TAYLOR, C. ZIENKIEWICZ, *Finite Elements in Fluids - Volume 2: Mathematical Foundations, Aerodynamics and Lubrication*, Wiley-Interscience Publication, 1975.
- [31] R. G. GHANEM AND P. D. SPANOS, *Stochastic Finite Elements: A Spectral Approach*, Springer, New York, NY, 1991.
- [32] M. GILES AND L. SZPRUCH, *Multilevel Monte Carlo methods for applications in finance*, World Scientific, 2013, pp. 3–48.
- [33] M. B. GILES, *Multilevel Monte Carlo path simulation*, Operations research, 56 (2008), pp. 607–617,792.

- [34] M. B. GILES, *Multilevel Monte Carlo methods*, Acta Numerica, 24 (2015), p. 259–328.
- [35] M. B. GILES AND L. SZPRUCH, *Antithetic multilevel Monte Carlo estimation for multi-dimensional SDEs without Lévy area simulation*, The Annals of Applied Probability, 24 (2014), pp. 1585–1620.
- [36] I. G. GRAHAM, F. Y. KUO, J. A. NICHOLS, R. SCHEICHL, C. SCHWAB, AND I. H. SLOAN, *Quasi-Monte Carlo finite element methods for elliptic PDEs with lognormal random coefficients*, Numerische Mathematik, 131 (2015), pp. 329–368.
- [37] I. G. GRAHAM, F. Y. KUO, D. NUYENS, R. SCHEICHL, AND I. H. SLOAN, *Analysis of Circulant Embedding Methods for Sampling Stationary Random Fields*, SIAM Journal on Numerical Analysis, 56 (2018), pp. 1871–1895.
- [38] P. GRISVARD, *Singularities in Boundary Value Problems*, Springer Verlag, 1992. vol. 22 of Research notes in applied mathematics.
- [39] A.-L. HAJI-ALI, F. NOBILE, E. VON SCHWERIN, AND R. TEMPONE, *Optimization of mesh hierarchies in Multilevel Monte Carlo samplers*, Stochastics and Partial Differential Equations: Analysis and Computations, 4 (2016), pp. 76–112.
- [40] E. J. HALL, H. HOEL, M. SANDBERG, A. SZEPESSY, AND R. TEMPONE, *Computable error estimates for finite element approximations of elliptic partial differential equations with rough stochastic data*, SIAM Journal on Scientific Computing, 38 (2016), pp. A3773–A3807.
- [41] H. HARBRECHT, M. PETERS, AND R. SCHNEIDER, *On the low-rank approximation by the pivoted Cholesky decomposition*, Applied Numerical Mathematics, 62 (2012), pp. 428–440. Third Chilean Workshop on Numerical Analysis of Partial Differential Equations (WONAPDE 2010).
- [42] S. HEINRICH, *Monte Carlo Complexity of Global Solution of Integral Equations*, Journal of Complexity, 14 (1998), pp. 151–175.
- [43] S. HEINRICH AND E. SINDAMBIWE, *Monte Carlo complexity of parametric integration*, Journal of Complexity, 15 (1999), pp. 317–341.
- [44] L. HERRMANN AND C. SCHWAB, *Multilevel quasi-Monte Carlo integration with product weights for elliptic PDEs with lognormal coefficients*, ESAIM: M2AN, 53 (2019), pp. 1507–1552.
- [45] H. HOEL AND S. KRUMSCHEID, *Central limit theorems for multilevel Monte Carlo methods*, Journal of Complexity, 54 (2019), pp. 101407, 16.
- [46] H. HOEL, E. VON SCHWERIN, A. SZEPESSY, AND R. TEMPONE, *Adaptive Multi Level Monte Carlo Simulation*, in Numerical Analysis of Multiscale Computations, vol. 82 of Lecture Notes in Computational Science and Engineering, Springer–Verlag, Berlin Heidelberg, 2011, pp. 217–234.

- [47] H. HOEL, E. VON SCHWERIN, A. SZEPESSY, AND R. TEMPONE, *Implementation and analysis of an adaptive multilevel Monte Carlo algorithm*, Monte Carlo Methods and Applications, 20 (2014), pp. 1–41.
- [48] T. J. HUGHES, *The finite element method: linear static and dynamic finite element analysis*, Courier Corporation, 2012.
- [49] C. JOHNSON, *Numerical solution of partial differential equations by the finite element method*, Studentlitteratur, Lund, 1987.
- [50] J. KARLSSON, S. LARSSON, M. SANDBERG, A. SZEPESSY, AND R. TEMPONE, *An error estimate for symplectic Euler approximation of optimal control problems*, SIAM Journal on Scientific Computing, 37 (2015), pp. A946–A969.
- [51] A. KEBAIER, *Statistical Romberg extrapolation: a new variance reduction method and applications to options pricing*, Annals of Applied Probability, 14 (2005), pp. 2681–2705.
- [52] K. KERGRENE, S. PRUDHOMME, L. CHAMOIN, AND M. LAFOREST, *A new goal-oriented formulation of the finite element method*, Computer Methods in Applied Mechanics and Engineering, 327 (2017), pp. 256–276. Advances in Computational Mechanics and Scientific Computation—the Cutting Edge.
- [53] R. KORNUBER AND E. YOUETT, *Adaptive Multilevel Monte Carlo Methods for Stochastic Variational Inequalities*, SIAM Journal on Numerical Analysis, 56 (2018), pp. 1987–2007.
- [54] F. KUO, R. SCHEICHL, C. SCHWAB, I. SLOAN, AND E. ULLMANN, *Multilevel quasi-Monte Carlo methods for lognormal diffusion problems*, Mathematics of Computation, 86 (2017), pp. 2827–2860.
- [55] J. LANG, R. SCHEICHL, AND D. SILVESTER, *A fully adaptive multilevel stochastic collocation strategy for solving elliptic PDEs with random data*, Journal of Computational Physics, 419 (2020), p. 109692.
- [56] Z. LI AND T. LU, *Singularities and treatments of elliptic boundary value problems*, Mathematical and Computer Modelling, 31 (2000), pp. 97–145.
- [57] A. LITVINENKO, Y. SUN, M. G. GENTON, AND D. E. KEYES, *Likelihood approximation with hierarchical matrices for large spatial datasets*, Computational Statistics & Data Analysis, 137 (2019), pp. 115–132.
- [58] Y. LIU, J. LI, S. SUN, AND B. YU, *Advances in Gaussian random field generation: a review*, Computational Geosciences, 23 (2019), pp. 1011–1047.
- [59] G. J. LORD, C. E. POWELL, AND T. SHARDLOW, *An Introduction to Computational Stochastic PDEs*, Cambridge Texts in Applied Mathematics, Cambridge University Press, 2014.

- [60] D. MCLEISH, *A general method for debiasing a Monte Carlo estimator*, Monte Carlo Methods Appl., 17 (2011), pp. 301–315.
- [61] M. S. MOMMER AND R. STEVENSON, *A goal-oriented adaptive finite element method with convergence rates*, SIAM journal on numerical analysis, 47 (2009), pp. 861–886.
- [62] K.-S. MOON, A. SZEPESSY, R. TEMPONE, AND G. E. ZOURARIS, *Convergence rates for adaptive approximation of ordinary differential equations*, Numerische Mathematik, 96 (2003), pp. 99–129.
- [63] ———, *Convergence rates for adaptive weak approximation of stochastic differential equations*, Stoch. Anal. Appl., 23 (2005), pp. 511–558.
- [64] K.-S. MOON, E. VON SCHWERIN, A. SZEPESSY, AND R. TEMPONE, *An Adaptive Algorithm for Ordinary, Stochastic and Partial Differential Equations*, in Recent Advances in Adaptive Computation, vol. 383 of Contemporary Mathematics, Providence, 2005, American Mathematical Society, pp. 325–343.
- [65] ———, *Convergence Rates for an Adaptive Dual Weighted Residual Finite Element Algorithm*, BIT Numerical Mathematics, 46 (2006), pp. 367–407.
- [66] A. MORAES, R. TEMPONE, AND P. VILANOVA, *Hybrid chernoff tau-leap*, Multiscale Modeling & Simulation, 12 (2014), pp. 581–615.
- [67] A. MORAES, R. TEMPONE, AND P. VILANOVA, *A Multilevel Adaptive Reaction-splitting Simulation Method for Stochastic Reaction Networks*, SIAM Journal on Scientific Computing, 38 (2016), pp. A2091–A2117.
- [68] D. T. P. NGUYEN AND D. NUYENS, *MDFEM: Multivariate decomposition finite element method for elliptic PDEs with lognormal diffusion coefficients using higher-order QMC and FEM*, ESAIM: M2AN, 55 (2021), pp. 1461–1505.
- [69] J. T. ODEN, *Finite Elements : Introduction*, Handbook of Numerical Analysis Volume II : Finite Element Methods (Part1), (1991).
- [70] ———, *Optimal h-p finite element methods*, Computer Methods in Applied Mechanics and Engineering, 112 (1994), pp. 309–331.
- [71] ———, *Adaptive multiscale predictive modelling*, Acta Numerica, 27 (2018), p. 353–450.
- [72] J. T. ODEN, I. BABUŠKA, AND D. FAGHIHI, *Predictive Computational Science: Computer Predictions in the Presence of Uncertainty*, John Wiley & Sons, Ltd, 2017, pp. 1–26.

- [73] J. T. ODEN, L. DEMKOWICZ, W. RACHOWICZ, AND T. A. WESTERMANN, *Toward a universal h-p adaptive finite element strategy, part 2. A posteriori error estimation*, Computer Methods in Applied Mechanics and Engineering, 77 (1989), pp. 113–180.
- [74] J. T. ODEN AND S. PRUDHOMME, *New approaches to error estimation and adaptivity for the Stokes and Oseen equations*, International journal for numerical methods in fluids, 31 (1999), pp. 3–15.
- [75] ———, *Goal-oriented error estimation and adaptivity for the finite element method*, Computers & Mathematics with Applications, 41 (2001), pp. 735–756.
- [76] J. T. ODEN AND S. PRUDHOMME, *Estimation of Modeling Error in Computational Mechanics*, Journal of Computational Physics, 182 (2002), pp. 496–515.
- [77] J. T. ODEN, S. PRUDHOMME, AND L. DEMKOWICZ, *A posteriori error estimation for acoustic wave propagation problems*, Archives of Computational Methods in Engineering, 12 (2005), pp. 343–389.
- [78] J. T. ODEN AND J. N. REDDY, *An introduction to the mathematical theory of finite elements*, Courier Corporation, 2012.
- [79] J. T. ODEN AND K. S. VEMAGANTI, *Estimation of Local Modeling Error and Goal-Oriented Adaptive Modeling of Heterogeneous Materials: I. Error Estimates and Adaptive Algorithms*, Journal of Computational Physics, 164 (2000), pp. 22–47.
- [80] C. PIAZZOLA AND L. TAMELLINI, *The Sparse Grids Matlab kit - a Matlab implementation of sparse grids for high-dimensional function approximation and uncertainty quantification*, ArXiv, (2022). 10.48550/ARXIV.2203.09314.
- [81] S. PRUDHOMME AND J. T. ODEN, *On goal-oriented error estimation for elliptic problems: application to the control of pointwise errors*, Computer Methods in Applied Mechanics and Engineering, 176 (1999), pp. 313–331.
- [82] ———, *Computable Error Estimators and Adaptive Techniques for Fluid Flow Problems*, in Error Estimation and Adaptive Discretization Methods in Computational Fluid Dynamics, T. J. Barth and H. Deconinck, eds., Springer Berlin Heidelberg, 2003, pp. 207–268.
- [83] W. RACHOWICZ, J. T. ODEN, AND L. DEMKOWICZ, *Toward a universal h-p adaptive finite element strategy part 3. design of h-p meshes*, Computer Methods in Applied Mechanics and Engineering, 77 (1989), pp. 181–212.
- [84] C.-H. RHEE AND P. W. GLYNN, *Unbiased estimation with square root convergence for SDE models*, Operations Research, 63 (2015), pp. 1026–1043.

- [85] L. SCARABOSIO, B. WOHLMUTH, J. T. ODEN, AND D. FAGHIHI, *Goal-oriented adaptive modeling of random heterogeneous media and model-based multilevel Monte Carlo methods*, Computers & Mathematics with Applications, 78 (2019), pp. 2700–2718.
- [86] M. SCHEUERER, *Regularity of the sample paths of a general second order random field*, Stochastic Processes and their Applications, 120 (2010), pp. 1879–1897.
- [87] C. SCHWAB AND R. A. TODOR, *Karhunen–Loève approximation of random fields by generalized fast multipole methods*, Journal of Computational Physics, 217 (2006), pp. 100–122.
- [88] E. STEPHAN AND J. R. WHITEMAN, *Singularities of the Laplacian at corners and edges of three-dimensional domains and their treatment with finite element methods*, Mathematical Methods in the Applied Sciences, 10 (1988), pp. 339–350.
- [89] A. TECKENTRUP, R. SCHEICHL, M. GILES, AND E. ULLMANN, *Further analysis of multilevel Monte Carlo methods for elliptic PDEs with random coefficients*, Numerische Mathematik, 125 (2013), pp. 569–600.
- [90] D. TERPSTRA, H. JAGODE, H. YOU, AND J. DONGARRA, *Collecting performance data with PAPI-C*, in Tools for High Performance Computing 2009, 3rd Parallel Tools Workshop, Dresden, Germany, Springer, Berlin Heidelberg, 2010, pp. 157–173.
- [91] K. S. VEMAGANTI AND J. T. ODEN, *Estimation of local modeling error and goal-oriented adaptive modeling of heterogeneous materials: Part II: a computational environment for adaptive modeling of heterogeneous elastic solids*, Computer Methods in Applied Mechanics and Engineering, 190 (2001), pp. 6089–6124.
- [92] L. B. WAHLBIN, *On the Sharpness of Certain Local Estimates for $\overset{\circ}{H}^1$ Projections into Finite Element Spaces: Influence of a Reentrant Corner*, Mathematics of Computation, 42 (1984), pp. 1–8.
- [93] E. YUETT, *Adaptive Multilevel Monte Carlo Methods for Random Elliptic Problems*, PhD thesis, Freie Universität Berlin, 2018.